

# A Comprehensive Study of Intense Star Formation Bursts in Irregular and Compact Galaxies <sup>\*</sup>

J. Miguel Mas-Hesse<sup>1</sup> and Daniel Kunth<sup>2</sup>

<sup>1</sup> Laboratorio de Astrofísica Espacial y Física Fundamental - INTA, POB 50727, E-28080 Madrid, Spain; e-mail: mm@laeff.esa.es

<sup>2</sup> Institut d'Astrophysique de Paris, 98 bis Bd. Arago, F-75014 Paris, France; e-mail: kunth@iap.fr

Received December 1998 / Accepted March 1999

**Abstract.** We have analyzed the properties of the star formation episodes taking place in a sample of blue compact and irregular galaxies by comparing their multiwavelength observational properties with the predictions of evolutionary population synthesis models. This method has allowed us to constrain the age, star formation regime (instantaneous or extended) and Initial Mass Function (IMF) slope, as well as the shape and strength of the interstellar extinction in these regions. We find that star formation episodes are essentially short with a mean age of 3.5 Myrs. Some galaxies may be undergoing their first global episode of star formation while for the rest of the sample older stars contribute to at most half the optical emission. The Wolf-Rayet star population (WR) is well reproduced by the models and provides the strongest argument in favor of a short duration of the star formation episode. Supernova rates are relatively large. The accumulation of supernova explosions within few Myr has contributed to a quick metal enrichment of the ISM and to its disruption by the release of huge amounts of mechanical energy.  $V - K$  colors agree well with the prediction that red supergiant stars are rare in low metallicity regions. A general agreement is found between the predicted and observed far infrared emissions suggesting that the fraction of hidden stars contributing to the ionisation is minimum, except in some specific objects. A saillant result of this study is that the IMF slope appear to be very universal, on average very close to that of the solar neighborhood and with no dependence on the metallicity, contrary to previous claims. We have also found no dependence whatsoever between the shape of the extinction law and the metallicity. It is likely that the strong radiation associated to the bursts destroys the dust component responsible for the 2175 Å bump. Finally we confirm that extinction affecting the stellar continuum is in some cases significantly weaker than that derived from the Balmer emission lines. Such a discrepancy can lead to underestimations in the value of the  $H\beta$  equivalent width by a factor as large as 2, leading to an over-

estimation of the age of the burst. Similarly, the Wolf-Rayet bump to the  $H\beta$  luminosities ratio can also be affected by this differential reddening leading to an overestimation of the WR star population. As bursts get older they appear dustier, possibly as a result of dust ejection during the evolution of their most massive stars. Finally, we have found a serious general discrepancy between the predicted and the measured radio luminosities. While part of this discrepancy might be attributed to aperture mismatching in some cases, it points to the presence of additional radio sources not included in present evolutionary models.

**Key words:** Stars: Wolf-Rayet; Galaxies: ISM; Galaxies: luminosity function, mass function; Galaxies: starburst; Infrared: galaxies; Ultraviolet: galaxies

## 1. Introduction

With the launch of the HST we are now witnessing a new era that allows to analyze in detail nearby objects such as Galactic H II regions or 30 Dor in the LMC. Such studies permit to resolve and study individual stars in massive star clusters and obtain UV spectra of hot stars with metallicities that are not solar. These studies combined with follow up observations from 10-m class telescopes will bring an enormous knowledge about massive star formation and evolution processes and in particular direct informations about the IMF slope, as well as its lower and upper mass limits and velocity dispersion of individual star clusters. However, as one tackles with objects at larger distances, stars will remain unresolved and so any argument will still be based on global properties. In particular in the quest for primeval galaxies at very large redshift one must be prepared to identify them and a thorough knowledge of the properties of nearby starbursts is indeed mandatory. For this reason studies of massive star formation in nearby galaxies have received a great attention in the past years. In the UV the seminal paper of Meier & Terlevich (1981) has pointed out the possible resemblance of a primeval galaxy with some local blue compact galaxies that might be forming stars for the first time. Kinney et al. (1996) compiled a set of templates from the UV to the near infrared for galaxies of different kinds, includ-

Send offprint requests to: J. M. Mas-Hesse

<sup>\*</sup> Based on observations from the *International Ultraviolet Explorer* obtained at the ESA VILSPA observatory, on observations taken at the Isaac Newton Telescope at the Spanish Observatorio del Roque de Los Muchachos on La Palma island and on observations with the Nançay radiotelescope.

ing starbursts, spirals and ellipticals, aiming to provide a way to properly apply K-corrections for high redshift objects. Very recently, Heckman et al. (1998) have presented a systematic study of the UV properties of a sample of 45 starburst and related galaxies, proposing to use them as a “training set” to better understand the properties of starbursts at high redshift. In parallel, efforts have been put in building various models using population synthesis techniques to reproduce all the observed electromagnetic spectrum from the UV up to X-rays (see the proceedings of the 1995 IAP (Kunth et al. 1996), 1995 Crete (Leitherer et al. 1996) and 1998 Puerto Vallarta (van der Hucht et al. 1998) conferences for a comparative compilation of synthesis models and observational results).

With these ideas in mind we started some years ago the detailed study of massive star formation episodes in different environments. The predictions of evolutionary populations synthesis models at various metallicities were presented and discussed in Arnault, Kunth & Schild (1989), Mas-Hesse & Kunth (1991a) and Cerviño & Mas-Hesse (1994). We now present a comprehensive observational study of massive star-formation episodes taking place in star-forming galaxies and Giant H II regions in nearby spiral galaxies. Preliminary partial results have been discussed in Mas-Hesse (1990) and Mas-Hesse & Kunth (1991b, 1996a,b). Our analysis is based on the integrated emission from the whole massive star clusters. The sample comprises a set of galaxies with different morphological types, luminosities and hosting environments. Some of them are close enough to have been recently studied with the HST, allowing comparisons to be made, while others are far more distant and remain suited for integrated studies like the present one or for statistical investigations. Our goal is to characterize what are the universal properties of starbursting episodes: Initial Mass Function (IMF), star formation regime (instantaneous or extended), evolutionary state, effects of dust particles, effects on the interstellar medium (ISM), etc... To achieve this, IUE UV data have been complemented with optical spectroscopical observations, with special care to match both apertures. The data set has been completed with IR, far infrared (FIR) and radio data. We will show that the comparison of multiwavelength observational data with the predictions of synthesis models is a powerful tool to constrain the properties of these star-forming episodes.

The observational data (optical, ultraviolet, FIR and radio) are described in Sect. 2; the predictions of our evolutionary models are presented in Sect. 3; the model fitting techniques require some subtle handling that critically depends on the quality and completeness of each available data set as exposed in Sect. 4; the results are given in Sect. 5, together with a complete discussion of the processes that govern fundamental starburst properties; in Sect. 6 we discuss in more detail the properties of some individual galaxies; our conclusions are finally summarized in Sect. 7.

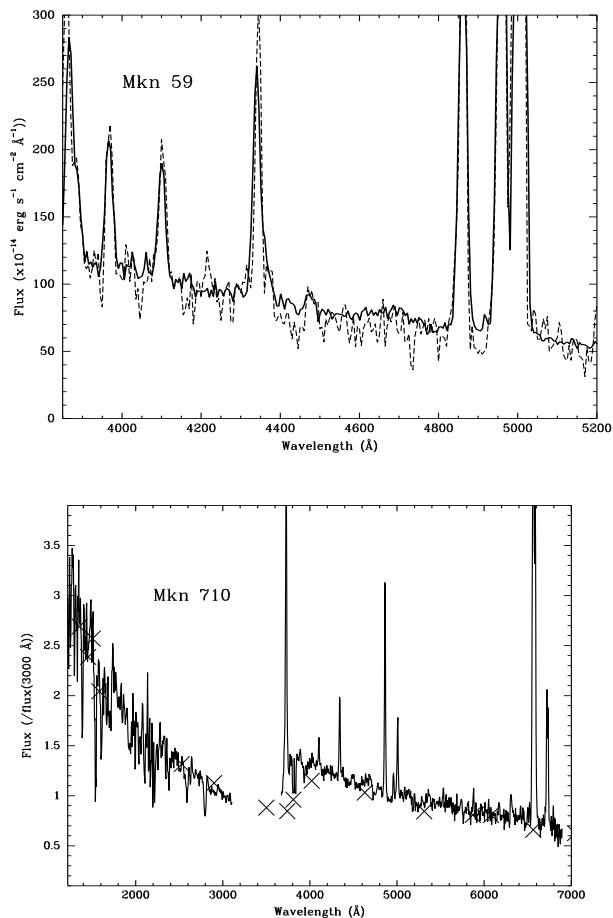


**Fig. 1.** a) Mrk 59 IPCS spectrum (solid line) over the corresponding CCD spectrum, both taken with  $10''$  broad slits. Note the good photometrical agreement between both spectra, obtained during different runs and with different detectors. b) UV – optical spectrum (crosses) of Mrk 710 from Storchi-Bergmann et al. (1995) over the IUE and optical spectra obtained by us (solid line). The agreement of the optical spectra is rather good, especially above  $4000 \text{ \AA}$  (the continuum of our optical spectrum is quite noisy below  $3900 \text{ \AA}$ ).

## 2. Observational data

We selected galaxies with H II-region-like emission-line spectra and with a strong UV continuum, so that they could be observed with IUE. 12 objects were taken from the IUE catalogue of extragalactic H II regions from Rosa et al. (1984), rejecting those observations with low signal-to-noise or with technical problems (saturation, read-out errors...). Haro 2, IZw 36 and NGC 4670 were included for comparison with previous results by other investigators. We also included Mrk 710 and NGC 3256. Mrk 710 is a starburst galaxy with an important population of Wolf-Rayet stars (Kunth & Schild 1986), which is interesting to test the age calibration based on other parameters. NGC 3256 is an ultraluminous IRAS galaxy ( $L_{FIR} \approx 2 \cdot 10^{45} \text{ erg s}^{-1}$ ), probably a “merger” (Graham et al. 1984),

**Table 1.** Adopted properties of the selected star-forming regions.  $H_0 = 75 \text{ km s}^{-1} \text{ Mpc}^{-1}$  has been assumed. Coordinates have been taken from the NASA Extragalactic Database (NED). Galactic  $E(B - V)$  values have been taken from Burstein & Heiles (1984).

Name	R.A. (1950.0)	Dec.	Distance (Mpc)	Morphology	$E(B - V)_{Galactic}$	Other names
NGC 588	01 29 58.5	+30 23 51	0.82 <sup>1</sup>	GH II	0.045	In M33
NGC 595	01 30 44.7	+30 26 08	0.82 <sup>1</sup>	GH II	0.045	In M33
NGC 2363	07 23 23.7	+69 17 33	3.0 <sup>1</sup>	IG	0.042	In NGC 2366
IZw 18	09 30 30.2	+55 27 49	10.7 <sup>2</sup>	BCDG	0.005	Mrk 116
Mrk 710	09 52 10.2	+09 30 32	17.9 <sup>3</sup>	SG	0.010	NGC 3049
Tol 3	10 04 18.2	-29 41 29	11.6 <sup>4</sup>	BCDG	0.062	NGC 3125
NGC 3256	10 25 43.4	-43 38 48	50.0 <sup>5</sup>	Merger	0.14	VV 065
Haro 2	10 29 22.7	+54 39 31	20.2 <sup>6</sup>	BCDG	0.0	Mrk 33
Mrk 36	11 02 15.6	+29 24 28	8.0 <sup>7</sup>	BCDG	0.0	Haro 4
NGC 4214	12 13 08.0	+36 36 22	6.4 <sup>8</sup>	IG	0.0	
IZw 36	12 23 50.5	+48 46 13	4.6 <sup>9</sup>	BCDG	0.0	Mrk 209
NGC 4670	12 42 49.9	+27 23 55	12.1 <sup>6</sup>	BCDG	0.005	Haro 9
Mrk 59	12 56 38.5	+35 06 56	11.7 <sup>6</sup>	IG	0.0	NGC 4861
NGC 5253	13 37 05.0	-31 23 30	4.1 <sup>10</sup>	IG	0.047	Haro 10
NGC 5471	14 02 42.7	+54 38 08	6.3 <sup>11</sup>	GH II	0.0	In M101
IIZw 70	14 48 55.1	+35 46 37	17.6 <sup>7</sup>	BCDG	0.0	Mrk 829
IC 4662	17 42 12.0	-64 37 18	4.0 <sup>12</sup>	IG	0.065	He 2-269

Notes- GH II: giant H II region; IG: irregular galaxy; BCDG: blue compact dwarf galaxy; SG: starburst galaxy.

Distance references- <sup>1</sup>Sandage & Tamman (1974a), <sup>2</sup>Kinman & Davidson (1981), <sup>3</sup>Mazzarella & Balzano (1986), <sup>4</sup>Joseph & Wright (1985), <sup>5</sup>Kunth & Sèvre (1986), <sup>6</sup>Huchra et al. (1983), <sup>7</sup>French (1980), <sup>8</sup>Sandage & Tamman (1974b), <sup>9</sup>Viallefond & Thuan (1983), <sup>10</sup>Saha et al. (1995), <sup>11</sup>Aaronson & Mould (1983), <sup>12</sup>Alloin & Sareyan (1974).

and was selected to analyze if its enormous FIR luminosity was due to a very intense starburst triggered by the collision.

We list in Table 1 the name, coordinates, distance and morphological type of the 17 objects included in our sample. Distances have been taken from the literature, as indicated in the table. When needed, they were corrected so that all of them are consistent with  $H_0 = 75 \text{ km s}^{-1} \text{ Mpc}^{-1}$ . The Galactic  $E(B - V)$  color excess derived by Burstein & Heiles (1984) for each galaxy is also listed in Table 1. Seven are blue compact dwarf galaxies, while other 5 are irregular galaxies. The sample is completed with three giant H II regions, a starburst nucleus and an ultraluminous IRAS galaxy for comparison.

We have compiled UV, optical, far infrared and radio data for the majority of the objects in the sample. We have combined data taken from the literature and from astronomical databases (IUE and IRAS) with new observations, in order to cover a spectral range as wide as possible.

### 2.1. Optical

The main goals of the optical observations were essentially:

- To get the continuum spectral distribution in the 3600–7000 Å range over the same aperture as IUE ( $10'' \times 20''$ ). Aperture mismatch would have made impossible to compare directly the UV and optical continua. Moreover, by using such a large aperture we generally covered the major part of the ionized regions, which are much more extended than the stellar clusters, allowing us to compare the spa-

tially integrated emission of the Balmer lines with model predictions. In some objects Balmer lines fluxes can be underestimated by more than a factor 10 if obtained through narrow slits only  $1''$  wide.

- To observe with good signal-to-noise ratio the continuum around 4650 Å, looking for broad emission lines which could be the signature of Wolf-Rayet stars.

Nine objects of the sample were observed in January and May 1988 with the 2.5 m Isaac Newton telescope at La Palma Observatory, using the Intermediate Dispersion Spectrograph on the Cassegrain focus. We summarize in Table 2 the log of optical observations.

The January 1988 observations were performed with an Image Photon Counting System (IPCS) and a 138.5 Å/mm grating, covering the spectral range 3600–7000 Å with 2.0 Å per 15 μm pixel. We used a WG360 filter to cut the incident radiation below 3600 Å, avoiding so the contamination of the red part of the spectrum by second-order light. We took care to limit the count rate below 0.2 cts/s by using the corresponding neutral density filters, since the IPCS loses linearity at higher frequencies. The slit width was set to  $\approx 10''$  in order to match the IUE aperture and cover most of the star-forming regions.

The data from May 1988 were obtained with a blue-coated GEC P8603 CCD detector and the same instrumental configuration, observing the range 3600–5300 Å with 3.0 Å per 22 μm pixel. With a slit width of 1.8'' and allowing for relatively long integration times we got well exposed continua in the region of the Wolf-Rayet features. We also took some spectra with a

**Table 2.** Log of optical observations. An WG3650 filter was used with the IPCS to minimize second order contamination at  $H\alpha$ .

Object	Date	Detector	Slit (")	Pos. angle (deg.)	Exp. time (s)	$\lambda$ range Å
IZw 18	23-01-88	INT+IPCS	10	135	1500	3500–7000
Mrk 710	22-01-88	INT+IPCS	10	30	1800	3500–7000
Tol 3	23-02-80	LC+RETI	1x2	–	4800	3500–6900
Haro 2	22-01-88	INT+IPCS	10	330	1200	3500–7000
	22-01-88	INT+IPCS	10	330	1300	3500–7000
	11-05-88	INT+CCD	2	330	4500	3600–5300
	12-05-88	INT+CCD	2	330	2500	3600–5300
	12-05-88	INT+CCD	10	330	600	3600–5300
Mrk 36	23-01-88	INT+IPCS	10	90	660	3500–7000
NGC 4214	22-01-88	INT+IPCS	10	120	600	3500–7000
	11-05-88	INT+CCD	2	285	3000	3600–5300
	12-05-88	INT+CCD	10	285	300	3600–5300
	12-05-88	INT+CCD	2	285	1500	4250–5950
IZw 36	23-01-88	INT+IPCS	10	90	2220	3500–7000
NGC 4670	22-01-88	INT+IPCS	10	100	1500	3500–7000
	11-05-88	INT+CCD	2	265	2800	3600–5300
	12-05-88	INT+CCD	10	265	360	3600–5300
Mrk 59	23-01-88	INT+IPCS	10	10	1200	3500–7000
	12-05-88	INT+CCD	10	10	300	3600–5300
	12-05-88	INT+CCD	2	10	2000	3600–5300
NGC 5253	31-01-84	LS+HDS	4x4	–	600	3500–5900
IIZw 70	11-05-88	INT+CCD	2	225	3700	3600–5300
	11-05-88	INT+CCD	10	225	1200	3600–5300

Notes- INT: Isaac Newton Telescope; LC: Las Campanas 2.5m telescope; LS: La Silla 3.6m telescope.

10'' slit to check the photometric calibration of the IPCS spectra taken in January. We finally completed the data sample with narrow slit data for Tol 3 and NGC 5253.

The data were reduced using the European Southern Observatory IHAP package using standard procedures which included flat field corrections, bias subtraction (CCD), geometrical distortion correction (IPCS), wavelength calibration, sky subtraction and conversion to absolute fluxes. Three standard stars were observed each night through a 5'' slit. The instrumental response curves derived were very stable, with differences smaller than 10%, so that we used a mean curve for each observing run. We compare in Fig. 1a the optical IPCS and CCD spectra of Mrk 59, both obtained through the same broad slit during different runs. The discrepancies between the IPCS and CCD spectra taken with the same slit were found in any case to be smaller than 10%, precision that can be assigned to our photometrical calibration. We performed a further check of our calibration by comparing our UV - optical spectra with those obtained by Storchi-Bergmann et al. (1995) and McQuade et al. (1995), also obtained through a broad slit consistent with the IUE aperture. In Fig. 1b we plot the data corresponding to Mrk 710. It can be seen that both calibrations are consistent, and that the optical spectra are similar (the UV spectra used by these authors are the same IUE ones obtained by us). The agreement is quite good above 4000 Å, while at shorter wavelengths the low sensitivity of the IPCS yielded quite noisy continua. The spectra were corrected from Galactic extinction taking the color excesses from Burstein & Heiles

(1984) and using the extinction law as parameterized by Seaton (1979). Spectra were finally centered to nominal wavelengths, considering that the observed wavelength of a line was affected not only by cosmological redshift, but also by the location of the object in the rather wide 10'' slit.

We list in Table 3 the intensity of several lines measured on the 10'' slit spectra. We also list the intensity of the Wolf-Rayet bump measured on the narrow slit spectra. This bump is a blend of broad stellar atmospheric emission lines: He II  $\lambda 4686$ , N V  $\lambda 4603$ ,  $\lambda 4619$ , N III  $\lambda 4634$ ,  $\lambda 4640$ ,  $\lambda 4642$ , C III  $\lambda 4650$  and C IV  $\lambda 4658$ , where the nitrogen emission lines are attributed to stars of the WN sequence and the carbon emission to WC sequence stars, respectively. The WR bump intensity has been obtained interpolating the continuum between 4600 and 4700 Å and integrating all the excess emission above. The contribution of obvious narrow nebular lines has been subtracted by fitting a gaussian. In any case, of equal importance is the very detection or non-detection of the bump, indicative of the presence of Wolf-rayet stars in the cluster.

A first estimation of the extinction was derived by comparing the observed ratios between some Balmer lines ( $H\alpha$  to  $H\delta$ ) and theoretical values computed by Osterbrock (1989). Significant discrepancies in the derived color excesses  $E(B - V)$  were found depending on the pair of lines selected. Similar discrepancies have already been found by other authors in the past (Kunth & Sargent, 1983; Campbell et al. 1986) and are usually attributed to stellar absorption lines contamination, with equivalent widths in the range 1–2 Å. For consistency with previous

**Table 3.** Optical observed and derived properties. We list here the full emission lines intensities for the objects we did observe. Otherwise, derived data have been taken from the literature.  $W(H\beta)$  and  $I(WR)/H\beta$  values are given as measured on the spectra, without any correction.

	NGC 588	NGC 595	NGC 2363	IZw 18	Mrk710	Tol 3	NGC 3256	Haro 2	Mrk 36
$I([O\ II]\lambda 3727)$	–	–	–	0.49	1.76	0.87	–	3.70	1.82
$I(H\delta)$	–	–	–	0.32	0.09	0.19	–	0.12	0.19
$I(H\gamma)$	–	–	–	0.48	0.36	0.39	–	0.37	0.39
$I([O\ III]\lambda 4363)$	–	–	–	0.04	–	0.04	–	–	0.09
$I(H\beta)$	–	–	–	1.00	1.00	1.00	–	1.00	1.00
$I([O\ III]\lambda 4959)$	–	–	–	0.60	0.13	1.95	–	0.62	1.54
$I([O\ III]\lambda 5007)$	–	–	–	2.06	0.40	5.76	–	2.14	5.05
$I(H\alpha)$	–	–	–	2.97	4.25	2.41	–	3.79	2.84
$I(WR\ \lambda 4650)$	–	–	–	0.0	0.24	0.09	–	0.15	0.0
$E(B - V)$	0.10 <sup>a</sup>	0.33 <sup>a</sup>	0.16 <sup>c</sup>	0.05	0.29	0.17	0.85 <sup>d</sup>	0.22	0.0
$L(H\beta)$ (obs.)	6.5 10 <sup>37b</sup>	1.4 10 <sup>38b</sup>	9.2 10 <sup>38c</sup>	1.3 10 <sup>39</sup>	6.7 10 <sup>39</sup>	1.1 10 <sup>39</sup>	1.1 10 <sup>41d</sup>	2.0 10 <sup>40</sup>	7.3 10 <sup>38</sup>
$L(H\beta)$ (dered.)	1.2 10 <sup>38</sup>	4.5 10 <sup>38</sup>	1.6 10 <sup>39</sup>	1.5 10 <sup>39</sup>	1.8 10 <sup>40</sup>	2.0 10 <sup>39</sup>	1.9 10 <sup>42</sup>	4.2 10 <sup>40</sup>	7.3 10 <sup>38</sup>
(erg/s)						(1.6 10 <sup>40d</sup> )			
$W(H\beta)$ (Å)	97 <sup>a</sup>	≈100 <sup>a</sup>	300 <sup>c</sup>	135	35	98	20 <sup>d</sup>	30	110
						(50 <sup>d</sup> )			
$O/H$	8.3	8.4	7.9	7.2	8.9	8.2	8.9	8.4	7.8
$T_{eff}$	36600	35000	42700	35000	39800	38200	37000	35400	40000
$L_{3000}$	9.66 10 <sup>35</sup>	9.50 10 <sup>35</sup>	1.94 10 <sup>37</sup>	3.70 10 <sup>37</sup>	1.97 10 <sup>38</sup>	2.22 10 <sup>38</sup>	1.20 10 <sup>40e</sup>	6.55 10 <sup>38</sup>	6.81 10 <sup>37e</sup>
(erg s <sup>-1</sup> Å <sup>-1</sup> )									

**Table 3.** Continuation.

	NGC 4214	IZw 36	NGC 4670	Mrk 59	NGC 5253	NGC 5471	IIZw 70	IC 4662
$I([O\ II]\lambda 3727)$	4.44	0.86	3.40	1.68	1.61	–	2.07	–
$I(H\delta)$	0.11	0.25	–	0.24	0.20	–	0.14	–
$I(H\gamma)$	0.38	0.62	0.40	0.40	0.41	–	0.42	–
$I([O\ III]\lambda 4363)$	–	–	–	–	0.04	–	–	–
$I(H\beta)$	1.00	1.00	1.00	1.00	1.00	–	1.00	–
$I([O\ III]\lambda 4959)$	1.02	1.99	1.11	2.03	1.75	–	1.29	–
$I([O\ III]\lambda 5007)$	3.21	6.82	3.29	6.82	5.62	–	3.69	–
$I(H\alpha)$	4.01	3.03	4.29	2.86	–	–	–	–
$I(WR\ \lambda 4650)$	0.25	–	≤0.1	0.08	0.03	0.02	0.0	0.005
$E(B - V)$	0.28	0.0	0.32	0.0	0.19	0.15 <sup>f</sup>	0.17	0.09 <sup>i</sup>
$L(H\beta)$ (obs.)	4.9 10 <sup>39</sup>	8.6 10 <sup>38</sup>	7.0 10 <sup>39</sup>	1.4 10 <sup>40</sup>	1.8 10 <sup>38</sup>	1.2 10 <sup>39g</sup>	7.8 10 <sup>39</sup>	1.6 10 <sup>39h</sup>
$L(H\beta)$ (dered.)	1.3 10 <sup>40</sup>	8.6 10 <sup>38</sup>	2.1 10 <sup>40</sup>	1.4 10 <sup>40</sup>	3.4 10 <sup>38</sup>	2.0 10 <sup>39</sup>	1.4 10 <sup>40</sup>	2.2 10 <sup>39</sup>
(erg/s)					(6.9 10 <sup>39d</sup> )			
$W(H\beta)$ (Å)	49	300	27	135	161	129 <sup>g</sup>	49	65 <sup>h</sup>
					(80 <sup>d</sup> )			
$O/H$	8.4	7.8	8.4	8.0	8.2	8.0	8.0	8.3
$T_{eff}$	37000	40000	37000	40000	37000	39000	36000	38000
$L_{3000}$	1.33 10 <sup>38</sup>	2.73 10 <sup>37e</sup>	3.36 10 <sup>38</sup>	2.83 10 <sup>38</sup>	1.12 10 <sup>38</sup>	6.84 10 <sup>37</sup>	2.74 10 <sup>38</sup>	6.37 10 <sup>37</sup>
(erg s <sup>-1</sup> Å <sup>-1</sup> )								

Notes and references: <sup>a</sup> Vílchez et al. (1988); <sup>b</sup> Melnick (1979), the slit comprises the whole H II region; <sup>c</sup> Peimbert et al. (1986), 4'' x 12'' slit; <sup>d</sup> Storchi-Bergmann et al. (1995), 10'' x 20'' slit; <sup>e</sup> continuum luminosity measured at 1900 Å; <sup>f</sup> Rosa & Benvenuti (1994); <sup>g</sup> Torres-Peimbert et al. (1989); <sup>h</sup> Alloin (1974), 47'' circular aperture; <sup>i</sup> Heydari-Malayeri et al. (1990).

works we have fixed the  $H\beta$  absorption equivalent width to 1 Å, and have estimated which correction were needed in the  $H\gamma$  and  $H\delta$  lines to derive an homogeneous color excess. We have found that assuming absorption equivalent widths in the range 1–4 Å, with a mean value of 1.8 Å, the same  $E(B - V)$

is derived independently of the pair of lines used. This value of  $E(B - V)$  has been listed in Table 3. The correction to the emission flux calculated in this way amounts in average to 2% for  $H\beta$ , 9% for  $H\gamma$  and 50% for  $H\delta$ .

**Table 4.** Measured Si IV and C IV absorption lines equivalent widths.

Object	$W(\text{Si IV})$ Å	$W(\text{C IV})$ Å	$W(\text{Si IV})/W(\text{C IV})$
NGC 588	0.7±0.4	5.0±1.0	0.14±0.14
NGC 595	3.1±0.8	5.7±0.4	0.54±0.10
NGC 2363	em	em	–
IZw 18	–	–	–
Mrk 710	6.0±1.0	8.5±0.6	0.71±0.10
Tol 3	1.8±0.3	4.0±0.5	0.45±0.12
NGC 3256	7.5±1.0	7.5±2.0	1.0±0.3
Haro 2	5.4±0.7	5.5±0.7	1.0±0.2
Mrk 36	0.6±0.1	3.0±0.5	0.20±0.15
NGC 4214	2.8±0.3	4.2±0.4	0.67±0.12
IZw 36	em	em	–
NGC 4670	4.1±0.4	5.0±0.6	0.82±0.15
Mrk 59	2.0±0.6	2.2±0.4	0.91±0.30
NGC 5253	2.2±0.4	3.7±0.5	0.59±0.17
NGC 5471	1.0±0.2	2.0±0.2	0.50±0.15
IIZw 70	1.2±0.2	4.0±0.6	0.30±0.10
IC 4662	2.9±0.5	2.9±0.5	1.0±0.3

Notes- em: absorption profiles contaminated by nebular emission.

Oxygen abundances had already been published by other authors in the past but have been recalculated for those galaxies we observed in the optical. The measured oxygen abundances are listed in Table 3. We have completed it with values taken from the literature. Effective temperatures were estimated following the method described in Cerviño & Mas-Hesse (1994), based on the presumed temperature dependence of the oxygen over  $H\beta$  lines ratios.

The optical spectroscopy was complemented with data given by Storchi-Bergmann et al. (1995), which were also taken through broad slits consistent with the IUE one.

## 2.2. Ultraviolet

We have compiled ultraviolet spectra taken with the International Ultraviolet Explorer (IUE) for all the galaxies in our sample. General information and references about IUE can be found in Kondo (1988). All these spectra were taken at low resolution ( $\approx 6$  Å) through an oval entrance aperture of approximately  $10'' \times 20''$ . The whole 1100–3200 Å spectral range is available for the majority of the galaxies except NGC 3256, Mrk 36 and IZw 36, for which only the short wavelength range has been observed.

We took the standard 2-dimensional line-by-line spectra distributed by the IUE observatory and reduced them using our own procedures. The steps involved were essentially defect pixels removal (hot pixels, cosmic rays, reseau marks), linear interpolation between adjacent pixels, background subtraction and photometric calibration. The accuracy of the IUE photometric calibration at low resolution is approximately 10%, consistent with the optical data accuracy. Spectra were shifted to set the red wing of the C IV absorption line at its nominal

wavelength. Optical redshifts were not used, since the large size of the entrance slit can imply a spectral shift of a few Å if the object is not well centered into the aperture. When more than one spectrum were available we coadded them to improve the signal-to-noise ratio. The spectra were finally corrected from galactic extinction using the Seaton (1979) law and  $E(B - V)$  color excesses derived by Burstein & Heiles (1984). We found no significant discrepancy between the spectra extracted by our procedure and those included in the catalogue of starburst galaxies by Kinney et al. (1993).

We have measured equivalent widths of the Si IV 1393+1403 and C IV 1548+1551 absorption lines following the prescriptions of Sekiguchi and Anderson (1987a). The continuum was defined by two 40-Å-wide clean intervals located within 80 Å on either side of the lines. The absorption and the emission features were identified as those parts below and above the linearly interpolated continuum level, respectively. Equivalent width of the Si IV and C IV absorption lines were then derived by integrating over the whole absorption feature. Since the lines have been measured consistently in the stars used in the Sekiguchi and Anderson (1987a) calibration and in our sample this procedure should be adequate. The continuum placement is certainly one of the largest source of systematic error in the equivalent widths measurements. We have estimated the errors by assigning various plausible continuum levels to the different features. An additional source of error is the contamination of the Si IV and C IV profiles by interstellar absorption lines, as well as by nebular emission lines. When the terminal velocity in the C IV line was higher than 3000 km/s we subtracted previously a gaussian fit to the Si II  $\lambda 1527$  interstellar line. The contamination of the profiles by interstellar Si IV and C IV absorption lines is expected to be weak, since most galaxies are metal deficient and little affected by extinction. Finally, in NGC 2363 and IZw 36 the nebular contamination completely prevented to measure the absorption lines. In the other galaxies the contamination by nebular emission seemed to be negligible. The measured equivalent widths with the corresponding errors are listed in Table 4. (The merged IUE and optical spectra will be discussed later and are displayed in Fig. 5).

## 2.3. Far Infrared

Except for IZw 18 and IZw 36 all other objects were detected by the Infrared Astronomical Satellite (IRAS) at 60 and/or 100  $\mu\text{m}$ . The IRAS angular resolution is around  $2'$  at 100  $\mu\text{m}$ , so that the measured fluxes include also the emission coming from surrounding regions. This is not a problem in the case of blue compact dwarf galaxies, in which star-forming regions clearly dominate over the entire galaxy. On the other hand, the measured flux will be strongly contaminated by emission unrelated to the star-forming episode in more extended objects, like Mrk 710.

The FIR parameter defined by Helou et al. (1988) is a convenient representation of the far infrared flux measured by IRAS from any source dominated by thermal emission peak-

**Table 5.** FIR and radio luminosities. IZw 18 and IZw 36 were not detected by IRAS. The upper limit indicated corresponds to the maximum flux expected according to the sensitivity of the IRAS detectors.

Object	IRAS source	$f_{60}$ (Jy)	$f_{100}$ (Jy)	$T_{dust}$ (K)	$L_{FIR}$ (erg/s)	$L_{radio}$ (Jy kpc <sup>2</sup> )	$\alpha_{radio}$ (6-20 cm)
NGC 588	01299+3023	1.0	≤5.4	–	≤ 1.2 10 <sup>40</sup>	–	–
NGC 595	F01307+3025	11.0	≤35.1	–	≤ 8.3 10 <sup>40</sup>	6.3 10 <sup>4a</sup>	≈0
NGC 2363	07233+6917	3.3	4.6	42	2.7 10 <sup>41</sup>	1.3 10 <sup>6b</sup>	≈0
IZw 18	–	–	–	–	< 6.5 10 <sup>41</sup>	2.3 10 <sup>6b</sup>	-0.12
Mrk 710	09521+0930	2.7	4.3	40	7.4 10 <sup>42</sup>	6.0 10 <sup>8</sup>	≈-0.8
Tol 3	10042-2941	5.0	6.5	44	5.3 10 <sup>42</sup>	5.9 10 <sup>6c</sup>	–
NGC 3256	10257-4338	94.6	121.6	45	1.9 10 <sup>45</sup>	1.3 10 <sup>9g</sup>	–
Haro 2	10293+5439	4.8	5.5	47	1.6 10 <sup>43</sup>	6.1 10 <sup>7b</sup>	-0.8
Mrk 36	F11022+2924	0.2	≤0.7	–	≤ 1.4 10 <sup>41</sup>	1.5 10 <sup>6b</sup>	–
NGC 4214	12131+3636	14.5	25.5	38	5.3 10 <sup>42</sup>	3.6 10 <sup>7</sup>	≈-0.4
IZw 36	–	–	–	–	< 9.4 10 <sup>40</sup>	2.5 10 <sup>6d</sup>	>-0.3
NGC 4670	12428+2724	2.4	4.0	40	3.1 10 <sup>42</sup>	1.5 10 <sup>7e</sup>	–
Mrk 59	12566+3507	1.8	2.4	44	2.0 10 <sup>42</sup>	4.8 10 <sup>6a</sup>	-0.6
NGC 5253	13370-3123	31.2	29.8	51	4.0 10 <sup>42</sup>	1.0 10 <sup>7f</sup>	-0.1
NGC 5471	14027+5438	1.8	2.5	42	6.0 10 <sup>41</sup>	4.0 10 <sup>6a</sup>	-0.2
IIZw 70	14489+3546	0.7	1.5	36	2.1 10 <sup>42</sup>	1.3 10 <sup>7d</sup>	-0.3
IC 4662	17422-6437	8.3	11.8	42	1.1 10 <sup>42</sup>	–	–

References: <sup>a</sup> Sramek & Weedman (1986); <sup>b</sup> Klein et al. (1984); <sup>c</sup> van Driel et al. (1991); <sup>d</sup> Wynn-Williams & Becklin (1986); <sup>e</sup> Huchra et al. (1983); <sup>f</sup> Beck et al. (1996); <sup>g</sup> Forbes & Ward (1993)

ing between 50 and 100  $\mu\text{m}$ , as is generally the case in star-forming regions. FIR estimates the flux measured between 42.5 and 122.5  $\mu\text{m}$  and is defined as

$$FIR = 1.26 \cdot 10^{-14} [2.58 f_{\nu}(60\mu\text{m}) + 1.00 f_{\nu}(100\mu\text{m})] \text{ Wm}^{-2}$$

where  $f_{\nu}(60\mu\text{m})$  and  $f_{\nu}(100\mu\text{m})$  are the nominal flux densities. The total far infrared flux has been estimated following the calibration of Helou et al. (1988): first we derived a mean dust temperature from the  $f_{\nu}(60\mu\text{m})/f_{\nu}(100\mu\text{m})$  ratio, assuming a dust emissivity index of 1. The total far infrared flux has then been extrapolated to the 1–1000  $\mu\text{m}$  band assuming a blackbody distribution. This estimation of the total far infrared flux is a lower limit since other cooler and/or hotter components have been neglected. Puget & Léger (1989) have shown for example that nearly 30% of the Galactic far infrared flux is emitted below 40  $\mu\text{m}$  by very small grains and large aromatic molecules, which contribute significantly to the UV extinction. Unfortunately, very few among our galaxies have been detected at 12 and 25  $\mu\text{m}$ , so that a two-temperature model is not generally possible. Mas-Hesse (1992) found analyzing a larger sample of BCG that in average 30% of the far infrared flux is emitted below 40  $\mu\text{m}$ , in good agreement with the results of Puget & Léger (1989). While the far infrared luminosity we have derived is only a lower limit the real value should not be therefore higher by much more than a factor 1.5. We list in Table 5 the estimated total far infrared luminosities.

#### 2.4. Radio

Mrk 71, Mrk 710, NGC 4214 and NGC 4670 were observed in July-August 1989 with the Nançay radiotelescope in the continuum at 21, 18 and 9 cm. Only Mrk 710 and NGC 4214 were detected at 21 and 18 cm, getting upper limits at 9 cm. Observations were performed by drifting, i.e., positioning the chariot with the antenna and keeping it fixed during source transit. Thanks to the length of the available tracks this procedure could be repeated every 2 minutes around 30 times each day. The data were processed at Nançay using the SIR package. We first integrated the signal received during all the cycles, rejecting those affected by external contamination (storms,...) and adding the four channels provided by the autocorrelator (2 for vertical and 2 for horizontal polarization). The baseline was then fitted by a polynomial and subtracted. A gaussian was finally fitted to the remaining signal and the total flux was evaluated. Two reference sources were observed for absolute calibration, C287 and C295 (Kühr et al., 1981). The measurements are summarized in Table 6. The accuracy of the photometric calibration lies between 10% at 21 cm and 20% at 9 cm. The quoted errors have been derived by assuming different baseline levels.

Radio continuum data for the rest of the sample have been taken from the literature. Fluxes at 6 cm are listed in Table 5 together with the radio spectral index. We stress again that these radio fluxes generally correspond to the integrated galaxy and not only to the star-forming regions.

### 3. Evolutionary synthesis models

Our evolutionary population synthesis models have been discussed in detail in Arnault et al. (1989), Mas-Hesse & Kunth

**Table 6.** Radio data taken at Nançay radiotelescope. The fluxes are given in mJy. Values within parentheses correspond to the reference fluxes of Kühr et al., 1981).

Object	$S_{21cm}$	$S_{18cm}$	$S_{9cm}$
C287	6.2 (7.1)	6.3 (6.3)	3.2 (4.1)
C295	24.9 (22.0)	21.0 (21.0)	11.3 (10.0)
Mrk 710	150±10	126±15	≤70
NGC 4214	70±25	65±25	≤50
NGC 4670	±18	–	±30

(1991a) and Cerviño & Mas-Hesse (1994). They are based on the set of stellar evolutionary tracks provided by the Geneva group (Schaller et al. 1992; Schaerer et al. 1993ab; Charbonnel et al. 1993), which have been computed for several metallicities between  $Z=2Z_{\odot}$  and  $Z=Z_{\odot}/20$ , including overshooting and taking into account the effect of the WR atmospheres on the emitted spectral energy distribution. Our models consider a stochastic IMF generated by the Monte Carlo method with initial masses between 2 and 120  $M_{\odot}$  and a power law dependence on mass  $\phi(m) = dN/dm \sim m^{-\alpha}$ . We have assumed three values for the slope, the Salpeter’s one,  $\alpha = 2.35$ , and two extreme values,  $\alpha = 1, 3$ . We have used very short time steps ( $\geq 0.05$  Myr) to account for very rapid stellar phases such as the WR one. Two extreme star formation regimes have been considered: an instantaneous burst (IB) and an extended episode (EB) at a constant star formation rate. Calculations have been performed for a period of only 20 Myr, since we were mainly interested in the evolution of the most massive stars. After this time, a constant star formation process enters an asymptotic phase in which the population of massive stars ( $M \geq 12 M_{\odot}$ ) is nearly constant. Our EB models should not be confused with those assuming constant star formation rates over several Gyr, since even at 20 Myr stars with masses below around 10 Myr have not yet left the Main Sequence.

The synthesis has been performed in two steps. We have first synthesized the population of massive stars in a young cluster as a function of age, IMF and metallicity. More precisely, we have calculated the number and luminosity (per unit solar mass formed) of stars of each spectral type (O3 to M5) and luminosity class (I, III and V) by mapping the HR diagram as the stars evolve along the evolutionary tracks. We have then computed a set of observational parameters covering the UV to radio range using a compilation of spectra and fundamental properties of standard stars of each type. Although this compilation is based only on solar metallicity stars, we have selected a set of observational parameters which, in principle, are not seriously affected by the metallicity of the corresponding stars. Our dependence on metallicity is then based solely on its effects on the stellar evolutionary tracks, which originate very different stellar populations at a given time. We have discussed in Mas-Hesse & Kunth (1991a) the limitations of this approach. Synthesis models based on stellar atmosphere models at different metallicities have been presented in the last years (García-Vargas et al. 1994; Schaerer & Vacca 1998). While these mod-

els provide a more accurate prediction of the shape of the ionizing continuum (and are thus better suited to synthesize the emission line spectrum), the parameters we have synthesized are not significantly affected. In the following paragraphs we will discuss briefly our set of parameters and their validity for constraining the properties of the star formation processes:

### 3.1. Ionizing flux and effective temperature

The number of ionizing photons can be measured from the luminosity of the Balmer emission lines and also from the thermal radio emission. There are essentially two technical problems: first, the extinction affecting the nebular gas in global has to be well determined and corrected. As we will see later, inhomogeneities in the dust particles distribution can make this task rather complex. It is also very difficult to account for the number of high energy photons directly absorbed by dust, which do not contribute to the ionization process. We have assumed as a first approximation that in average 30% of the photons below 912 Å are directly absorbed, as found in Galactic H II regions by Smith et al. (1978) and Mezger (1978), but the exact value will depend on each galaxy. Second, it is needed to integrate the emission line fluxes over the whole emitting region. If such region is ionization bounded and the flux is spatially integrated over the whole emitting region, the complete number of ionizing photons can be estimated. If this is not the case, a significant fraction of the photons could escape without being accounted for when comparing with models predictions. As explained above, we have measured  $L(H\beta)$  through a large slit in order to cover essentially the whole ionized regions and minimize these problems.

Effective temperatures provide an additional constraint on the mass distribution of stars that dominates the ionizing emission of the cluster. The effective temperature can not be directly measured but has to be estimated from its effects on several emission lines. Unfortunately, these effects are also very dependent on other properties of the nebular gas (filling factor, density, metallicity,...), which not always can be well determined. Effective temperature estimates therefore strongly depend on the photoionization scenario (see Vílchez & Pagel 1988 and Cerviño & Mas-Hesse 1994). The determination of the effective temperature can be in error if spatial integration of the emission flux over the whole region is not performed.

### 3.2. Spectral energy distribution (SED)

We have computed the spectral energy distribution in the UV, optical, near and far infrared and radio ranges. Each of these energy ranges can be dominated by different stellar populations, so that the comparison of the whole predicted and observed SEDs is a powerful method to set constraints on the structure of the stellar population. While the UV emission is dominated by young, hot stars, the principal contributors to the near infrared bands are red supergiant stars formed during the burst (or even nebular continuous emission, depending on the evolutionary state of the burst). The radio continuum is essentially



due to thermal emission when the burst is young, but can be dominated by the non-thermal emission of supernova remnants once the most massive stars have ended their lifetime. The principal problem is the contamination of the observed flux by an underlying population of older stars, unrelated to the present burst. While this problem is minimal in the UV range, it can seriously affect the optical and near infrared ranges, especially if an important population of red giants is present (Thuan 1983). We have minimized this effect by selecting objects with very strong UV continuum, expected to be dominated in most wavelengths by the emission from young massive stars. We will see later that, nevertheless, in some cases the contribution of stars not related to the burst is still significant.

Constraints that can be derived from the optical-UV SED are hampered by two facts: first, the UV slope varies very weakly with age during the first 10 Myr (Fig. 2a). Second, even low amounts of interstellar dust produce a significant reddening of the UV emission (Fig. 2b). The energy these dust particles absorb is reradiated thermally in the far infrared range, as computed in Mas-Hesse & Kunth (1991a). Therefore, by simultaneously analyzing the shape of the UV continuum and the far infrared emission we can estimate the amount of extinction and recover the original SED. As a by-product we derive important information about the shape and strength of the extinction law in these objects, as we will discuss later. It is thus crucial to build information from a wide wavelength range to properly derive the properties of the stellar population in the young clusters.

An additional problem when comparing the FIR and radio luminosities is that both have been generally obtained through very large apertures, covering essentially the whole galaxies. The comparison is only meaningful in compact galaxies, in which the contribution in these bands is dominated by the star-forming region.

### 3.3. Ratio of the Si IV $\lambda 1400$ and C IV $\lambda 1550$ absorption lines equivalent widths

The Si IV  $\lambda 1400$  and C IV  $\lambda 1550$  absorption lines provide a direct evidence for the presence of a massive stellar population. They frequently show a P Cygni profile, as seen in the UV spectra of individual stars in our Galaxy. Their ratio is very sensitive to the spectral type of stars dominating the cluster emission since it varies by more than a factor 10 between O6 and B1 and shows a significant luminosity effect (Sekiguchi & Anderson 1987a; Mas-Hesse & Kunth 1991a).  $W(\text{Si IV})/W(\text{C IV})$  can then provide a first estimate about the dominant stellar population independently on any evolutionary model assumption. The use of the equivalent width of these lines to derive information about the stellar content of the clusters was first introduced by Sekiguchi & Anderson (1987a+b). Mas-Hesse & Kunth (1991a) and Cerviño & Mas-Hesse (1994) have synthesized the  $W(\text{Si IV})/W(\text{C IV})$  ratio as a function of age, IMF and metallicity of the star-forming region. Robert, Leitherer and Heckman (1993) have synthesized the whole profiles of

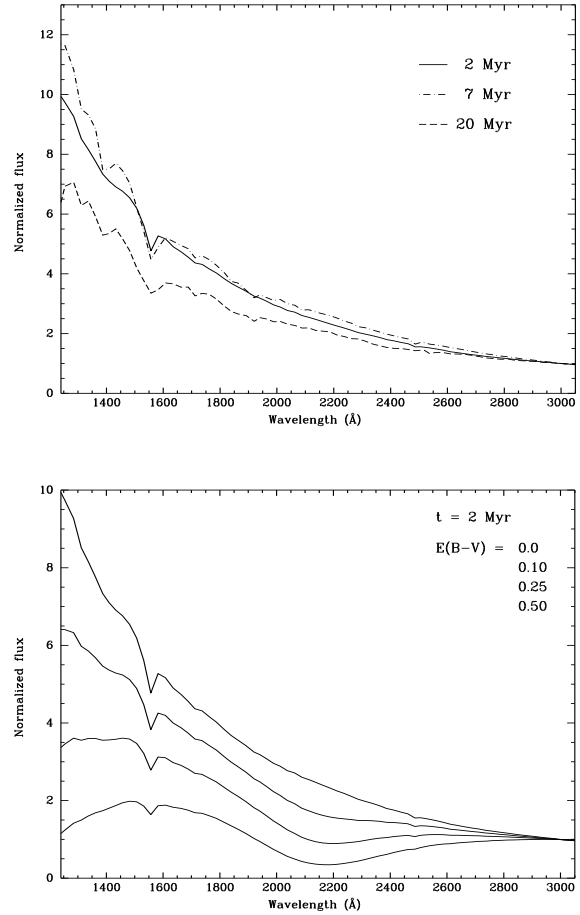


**Fig. 2.** a) Synthesized continuum spectra for different ages between 2 and 20 Myr. It can be seen that the UV slope varies weakly in the first 7 Myr, becoming even bluer than at zero age. b) Effects of interstellar extinction on a synthetic continuum of a 2 Myr old cluster. Even low amounts of dust modify significantly the shape of the UV continuum.

the lines for solar metallicity bursts based on a library of high resolution IUE spectra.

A major problem is that these equivalent widths strongly depend on the metallicity of the gas from which the stars formed. Profile fitting techniques or even approaches based on the analysis of single lines require the availability of a library matching the metallicity of the object under study. On the other hand, the ratio of both equivalent widths,  $W(\text{Si IV})/W(\text{C IV})$ , should be essentially independent on metallicity. We have plotted in Figs. 3a,b,c the measured  $W(\text{Si IV})$ ,  $W(\text{C IV})$  and  $W(\text{Si IV})/W(\text{C IV})$  versus the nebular oxygen abundance for the objects in our sample. It can be seen that the upper envelope of the  $W(\text{Si IV})$  and  $W(\text{C IV})$  vs. O/H distributions shows a clear trend toward lower strengths of Si IV and C IV absorption lines at low metallicities. The dispersion below this upper envelope is affected by evolutionary effects, since the lines become weaker when the cluster evolves. But the trend is weaker

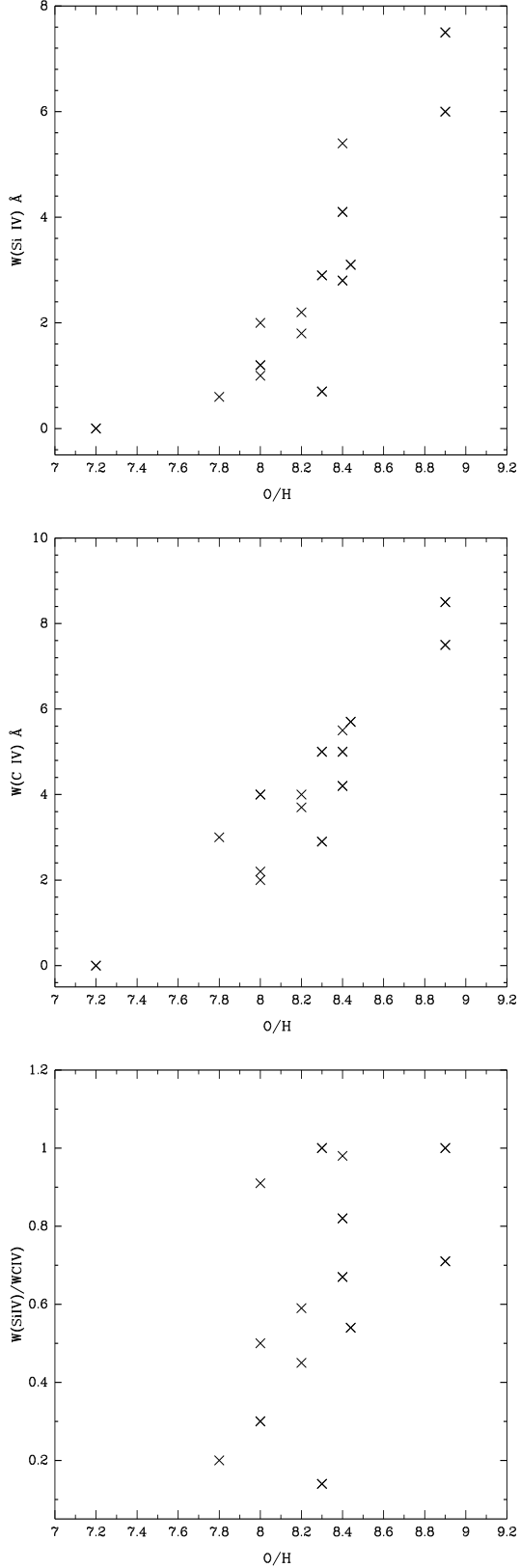


**Fig. 3.** a)  $W(\text{Si IV})$ , b)  $W(\text{C IV})$  and c)  $W(\text{Si IV})/W(\text{C IV})$  vs. the  $O/H$  abundance as measured from nebular emission lines for the objects in the sample.

or inexistent at all in the case of the  $W(\text{Si IV})/W(\text{C IV})$  ratio, as shown in Fig. 3c. Leitherer & Lamers (1991) have argued that the  $W(\text{Si IV})/W(\text{C IV})$  ratio could nevertheless be a function of the intrinsic metallicity of the stars. The effect should be negligible down to  $Z = Z_{\odot} / 3$ , but they predict an increase of the ratio at lower metallicities. Indeed, the Si IV line is expected to be a saturated photospheric line and therefore insensitive to  $Z$  while the C IV line would originate in the wind and therefore decrease with decreasing  $Z$ . Figs. 3a,b show that both lines are similarly sensitive to metallicity, contrary to predictions. In fact a clear upper envelope is well defined for both absorption lines, especially for C IV, which is generally stronger. This envelope defines the relative abundance of carbon and silicon with respect to oxygen in the gas from which the stars formed. A similar correlation between  $W(\text{Si IV})$  and  $W(\text{C IV})$  and the nebular oxygen abundance has been found by Storchi-Bergmann, Calzetti & Kinney (1994) in a sample of 44 star-forming galaxies.

As we pointed out in section 2, both the Si IV and C IV absorption lines of photospheric origin can be further contaminated by the additional contribution of interstellar absorptions adding a source of uncertainty in the determination of the  $W(\text{Si IV})/W(\text{C IV})$  ratio. In any case, the calibration of the  $W(\text{Si IV})/W(\text{C IV})$  ratio with spectral types already includes some degree of contamination by the Galactic ISM. HST allows to test to which extent the contribution by interstellar lines can dominate the  $W(\text{Si IV})/W(\text{C IV})$  ratio. From the comparison of the NGC 4214 HST spectra with synthetic ones presented by Leitherer et al. (1996), we can see that the effect of Si IV and C IV interstellar absorptions on the integrated equivalent widths of the P Cygni profiles is small and of the same order (or weaker) than the uncertainties induced by noise and by the placement of the continuum. We have therefore neglected this effect and assumed it is contained within our error bars.

### 3.4. $H\beta$ equivalent width

$W(H\beta)$  has been recognized for a long time as a very useful parameter to constrain the elapsed time since the onset of a star formation episode (Copetti et al. 1985; Melnick et al. 1985). Since it relates the number of the most massive stars ( $M > 20 M_{\odot}$ ) to lower mass ones it decreases continuously with time as the most massive stars cease to generate ionizing photons. Nevertheless, this age effect can be mixed with those induced by variations in the slope and upper mass limit of the IMF. Therefore, it is needed to compare simultaneously different parameters to constrain both the age and the IMF. This can be achieved for example by using the  $W(\text{Si IV})/W(\text{C IV})$  vs.  $W(H\beta)$  diagrams presented in Mas-Hesse & Kunth (1991a) and updated by Cerviño & Mas-Hesse (1994), as we will discuss later.

While  $W(H\beta)$  is in principle easy to measure on optical spectra there are a number of technical problems that can lead to erroneous results. First of all,  $W(H\beta)$  has to be measured over the complete region comprising all the stars that contribute to the continuum and also the whole  $H\beta$  emitted

flux. Since the extension of the ionized nebular gas is generally much larger than the region where the continuum is emitted,  $W(H\beta)$  can easily be underestimated. On the other hand, within a large aperture the contamination of the continuum by older stars might become important. Finally, the extinction may affect differently the nebular emission and the stellar continuum hence the determination of  $W(H\beta)$ . We will discuss later that in some cases the continuum seems to be significantly less reddened than the emission lines, contrary to the usual assumption that no such correction has to be applied to  $W(H\beta)$ .

### 3.5. The Wolf-Rayet bump strength

Wolf-Rayet stars are considered to be highly evolved descendants of the most massive O-stars. They are extreme Population I stars and have spectra characterized by broad emission lines resulting from dense, high-velocity winds. These stars are detectable in external galaxies by their prominent emission lines at around 4650-4690 Å (the “Wolf-Rayet bump”). This bump has been detected in many emission-line galaxies (Allen et al. 1976; Kunth & Sargent 1981, Kunth & Schild 1986; Conti 1991, Conti & Vacca 1992; Schaerer et al. 1999), providing a strong evidence that WR stars are indeed the descendants of massive O-type stars. Arnault et al. (1989), Cerviño & Mas-Hesse (1994), Meynet (1995) and Schaerer & Vacca (1998) have discussed the dependence of the WR bump strength on the parameters that define the star-forming episode (metallicity, age, IMF slope,...). The two most interesting properties of this feature are its strong dependence on metallicity and the constraints it can impose on the age of the cluster. Since the WR phenomenon is tightly coupled to the generation of strong stellar winds, its incidence decreases significantly with metallicity, so that at  $Z = Z_{\odot}/20$  only very massive stars (initial mass  $> 80 M_{\odot}$ ) might become WR. This small mass range implies that the detection of the WR bump in low metallicity galaxies can provide excellent on the upper mass limit of the IMF.

The relative population of WR over O stars is usually measured through the  $L(WR)/L(H\beta)$  ratio. To compare with model predictions it is again necessary to integrate over the whole ionized region. The observational measurements of this ratio might also be strongly affected by differential extinction. Since  $L(WR_{bump})$  is of stellar origin, it should be affected by the same extinction than the stellar continuum. On the other hand,  $L(H\beta)$  is of nebular origin and might suffer from a larger amount of extinction. Ignoring this effect may lead to a significant overestimation of the  $L(WR)/L(H\beta)$  ratio.

Finally, recent results by Cerviño (1998) show that if a significant fraction of massive stars are formed in binary systems, mass transfers episodes can lead to the formation of WR stars during longer periods of time than predicted by models based on the evolution of single stars alone. The age calibration through the WR features has to be therefore taken with caution.

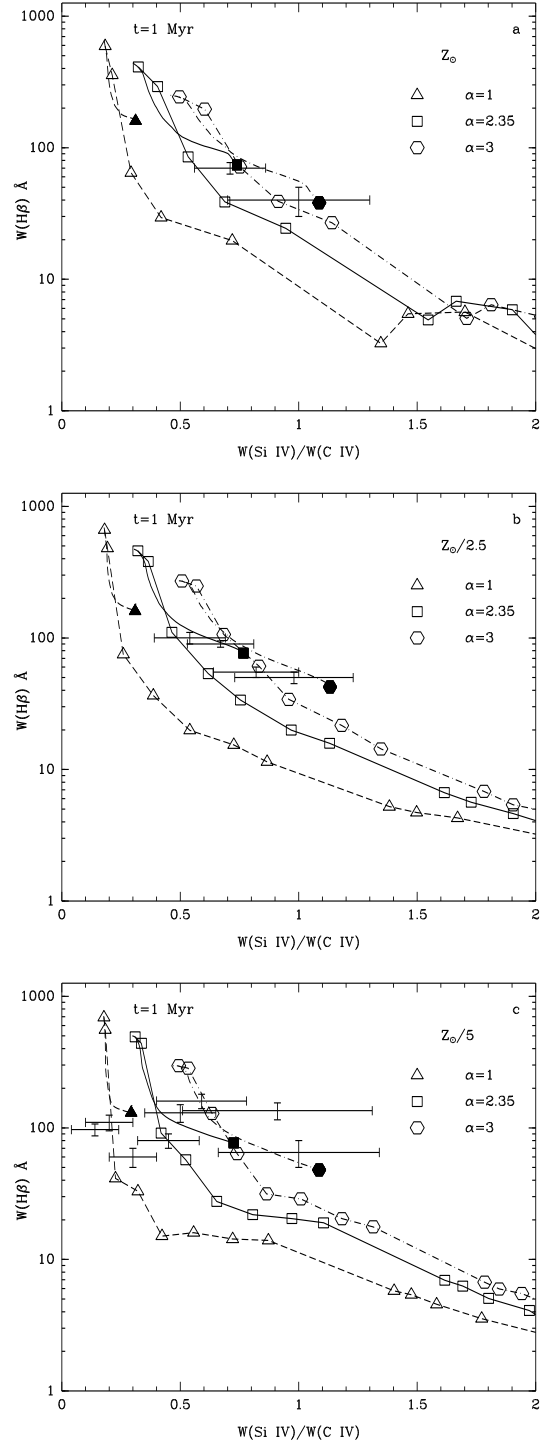


**Fig. 4.** Diagnostic diagrams  $W(H\beta)$  vs.  $W(Si\ IV)/W(C\ IV)$  ratio for different metallicities. The tracks have been computed for three IMF slopes, with a tick every 1 Myr. Solid symbols correspond to the asymptotic predictions for continuous star formation processes at 20 Myr. The observational values from the objects in our sample have been included with estimated error bars.

#### 4. Model fitting

It is clear from the above discussion that no single observable taken alone can constrain the properties of star forming processes. Only by simultaneously fitting several parameters over a large wavelength range tight to different physical processes can we optimize the unicity of the results. To fit the predictions of the evolutionary synthesis models to the observational data we rely upon the following steps (additional details on the fitting technique are given in Mas-Hesse & Kunth 1991a):

- i.- The diagnostic diagrams  $W(H\beta)$  vs.  $W(\text{Si IV})/W(\text{C IV})$  (Fig. 4) provide a first constraint on both the IMF slope and the age of the cluster (Cerviño & Mas-Hesse, 1994). Since they are metallicity dependent, we have used the O/H nebular abundance as an input value. Although the evolution of instantaneous or extended star formation episodes is significantly different, it is generally not possible to discriminate between both modes from these diagrams alone. For galaxies with no available  $W(\text{Si IV})/W(\text{C IV})$  ratio we assumed a Salpeter's IMF and used  $W(H\beta)$  for constraining the age.
- ii.- The age has been further constrained by the Wolf-Rayet bump. The  $L(WR)/L(H\beta)$  ratio is sensitive to the star formation regime (instantaneous or extended). On the other hand, when available, the radio spectral index has been used to disentangle between instantaneous or extended bursts. As discussed in Mas-Hesse & Kunth (1991a), the number of ionizing photons emitted in a burst in which new massive stars are being continuously formed is so high, that radio emission is always dominated by the thermal contribution from nebular gas, while the non-thermal fraction associated to supernova remnants is almost negligible. The detection of radio spectral indexes below  $\alpha = -0.5$  allows to reject extended star formation episodes. Since the radio emission is integrated over the whole galaxy, this constraint is reliable only for small objects dominated by the starburst, but not for larger galaxies with important disk population.
- iii.- We have fitted the UV continuum by models normalized at 3000 Å. We have selected 11 bands between 1285 and 3000 Å chosen to be relatively free from emission or absorption lines to perform the fitting. When only the 1200-1900 Å IUE range was available, 8 points were selected and the normalization was done at 1930 Å. The fitting has been performed assuming three different extinction laws: Galactic (Cardelli et al. 1991), Large Magellanic Cloud (LMC) (Nandy et al. 1981) and Small Magellanic Cloud (SMC) (Prévoit et al. 1984). The fit is qualified by the  $\epsilon$  parameter, which measures the deviation between the synthetic and the observed averaged continua.  
After these first three steps of the fitting procedure we ended with a relatively narrow range of valid models, as well as with an optimal extinction law and the corresponding value of the  $E(B - V)$  color excess.
- iv.- Comparing the observed luminosity at 3000 (1930) Å with the one predicted by the best models we derived the total amount of gas transformed into gas since the beginning of the burst (predictions are normalized to  $1 M_{\odot}$ ). This mass

corresponds to stars within the IMF boundaries ( $2-120 M_{\odot}$  and the corresponding slope). Once this normalization factor has been derived, we have computed model predictions for absolute parameters, like  $L_{FIR}$  and  $L(H\beta)$ .  $L_{FIR}$ , which is a function of the total reddening affecting the intrinsic UV SED, has then been compared to the observational value as a consistency check of the assumed extinction correction. A final constraint is provided by comparing observed and predicted  $H\beta$  luminosities. When available we have used  $H\beta$  luminosities observed through apertures similar to the IUE ones.

- v.- We have finally compared predicted and observed optical continua (only for those objects observed through large apertures). While in a burst dominated object the contribution to the optical continuum by an older underlying population should be negligible, this contribution can be important in some galaxies. Subtracting the predicted from the observed continuum flux we have estimated this contribution and have corrected the measured  $W(H\beta)$  value from the contamination by underlying population. With this corrected value of  $W(H\beta)$  we have iterated again at step i.

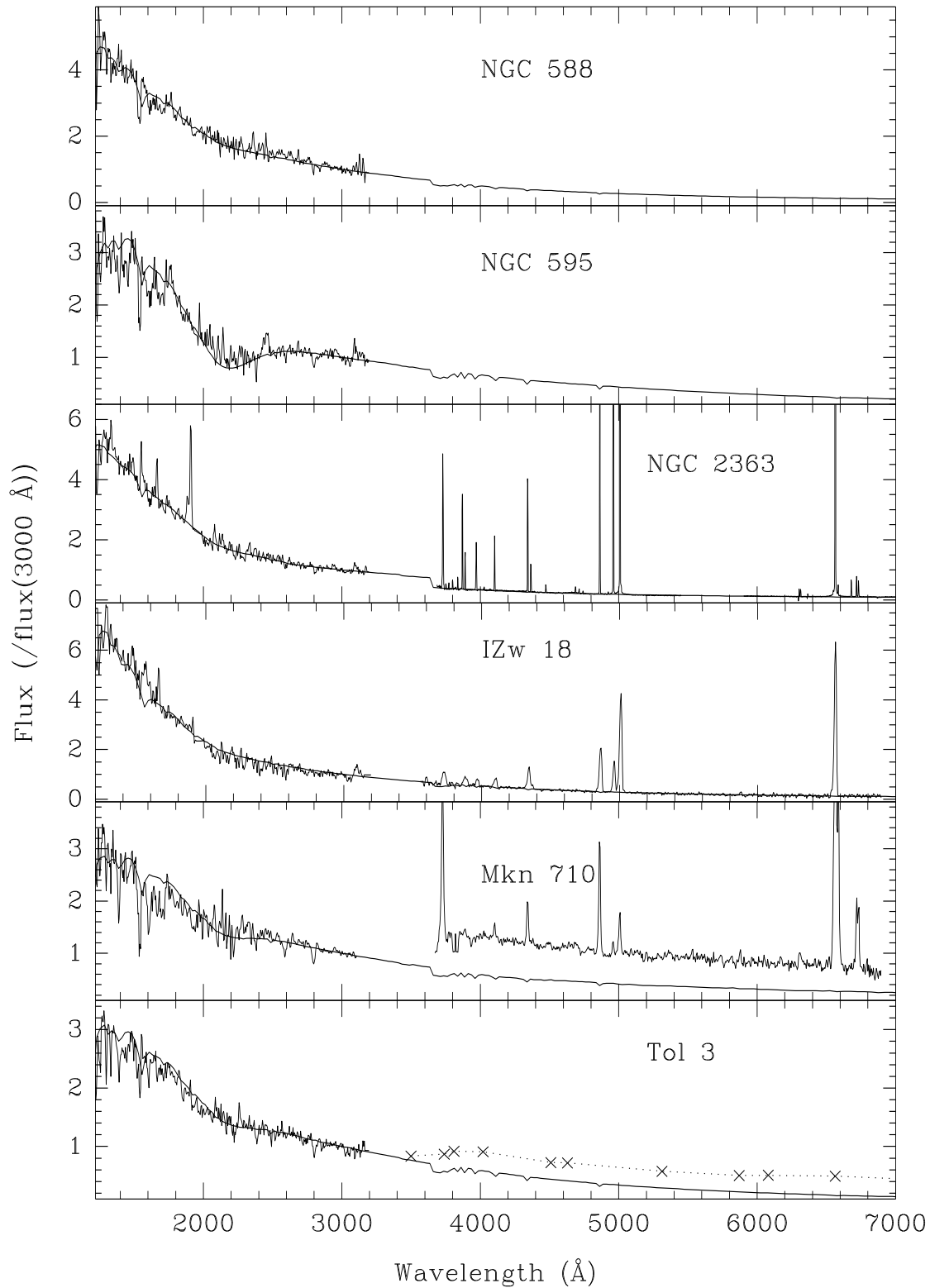
#### 5. Results and discussion

We have summarized in Table 7 the results of our evolutionary synthesis models applied to 17 star-forming regions. We list in this table the parameters that provide the best fit, together with their corresponding predicted and measured values. The mass of gas transformed into stars corresponds in all cases to the whole IMF range between 2 and  $120 M_{\odot}$ . This value does not necessarily correspond to the total amount of gas transformed into stars, since a significant fraction of gas is expected to have formed lower mass stars, not included in our computations. On the other hand, if the IMF is truncated at upper mass limits lower than  $120 M_{\odot}$ , the total mass involved would be correspondingly lower. We can see from the table that in general a solution can be found which simultaneously reproduces the whole set of multiwavelength parameters. Nevertheless, as we will discuss later, in some individual cases either the solution is not unique or some of the parameters can not be properly reproduced by the models.

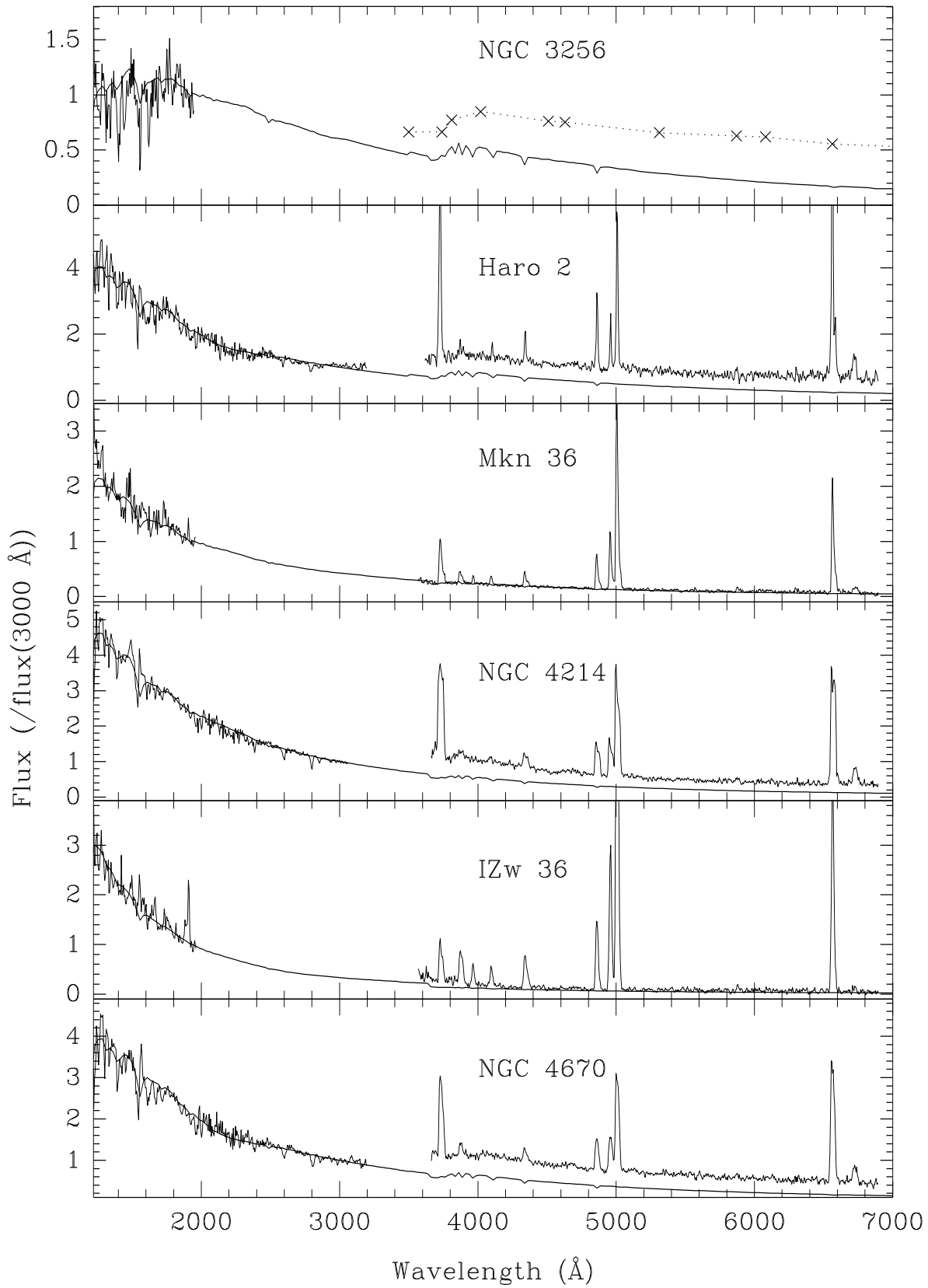
The observational values of  $W(H\beta)$  and  $L(WR)/L(H\beta)$  have been corrected from the contribution to the optical continuum of underlying older stars, as well as from differential extinction between continuum and emission lines, as explained below. We have plotted in Figs. 5 the continuum corresponding to the best fitting models over the observed IUE and optical spectra of the different objects. In Figs. 6,7 and 8 we show the comparison between the predicted and observational values of  $W(H\beta)$ ,  $W(\text{Si IV})/W(\text{C IV})$  and  $L(H\beta)$ .

##### 5.1. Age and star formation regime

The star formation regime seems to vary from object to object. While there are strong constraints in few objects toward constant star formation rates during at least 10-15 Myr, in most



**Fig. 5.** Synthetic over observational spectra of the different galaxies in the sample. Crosses and dotted lines correspond to the optical spectroscopy taken from Storchi-Bergmann et al. (1995). In those cases with optical spectra taken through narrow slits (see the text), the optical continuum has been normalized to the predicted flux. The optical range from NGC 5471 is a FOS spectrum provided by Rosa & Benvenuti (1994). The optical spectrum of NGC 2363 has been provided by R. González-Delgado and E. Pérez.

**Fig. 5.** Continuation.

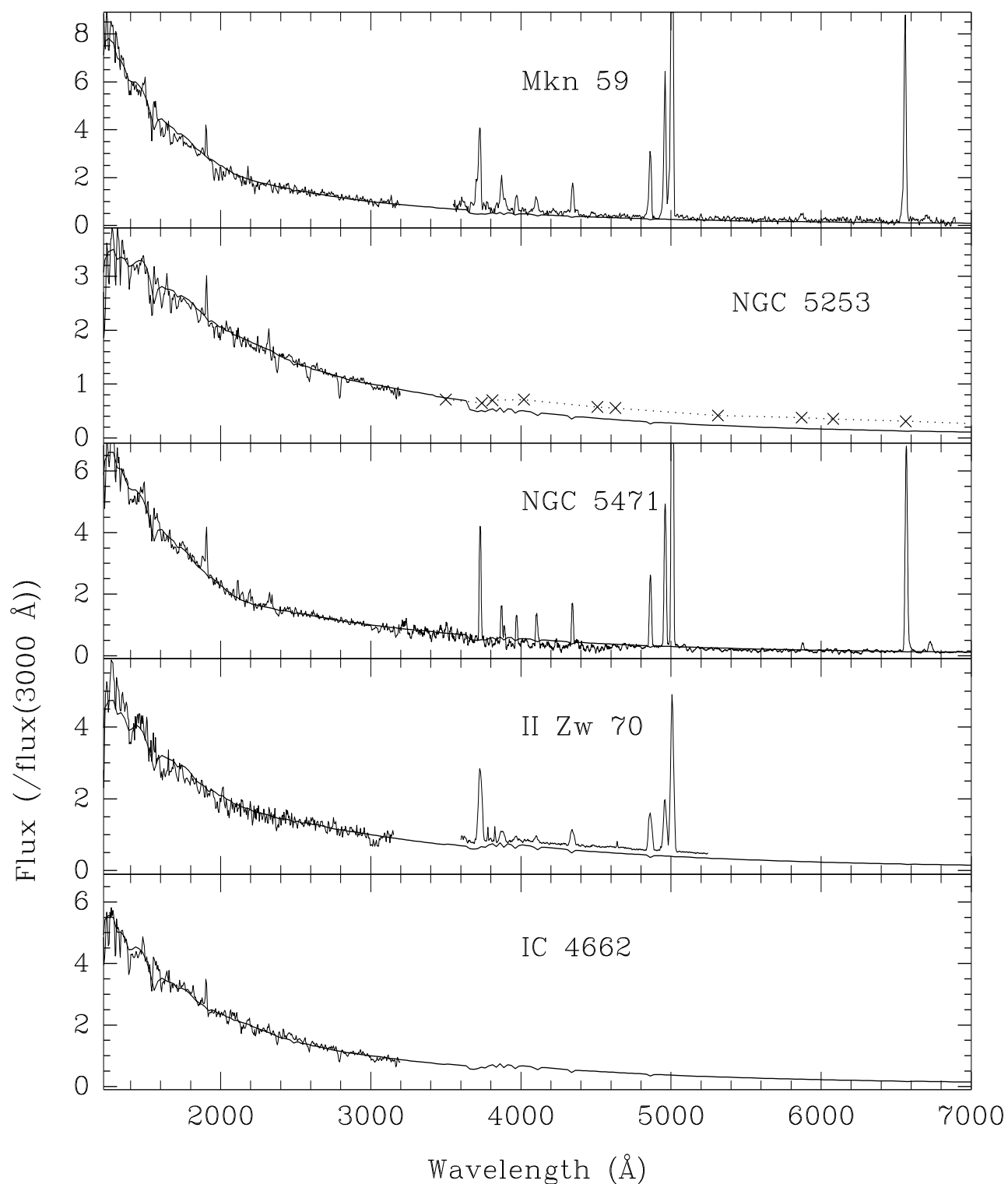


**Fig. 5.** *Continuation.*

cases the formation of massive stars seems to have been essentially coeval, as found in galaxies hosting large numbers of WR stars. Unfortunately, evolutionary synthesis models predict similar values for several parameters 3-5 Myr after an instan-

taneous burst and after 20 Myr of continuous star formation (Mas-Hesse & Kunth 1991a). For the purposes of this paper we have assumed in these ambiguous cases that the star formation episodes have been nearly instantaneous.

**Table 7.** Predicted vs. observational parameters. We have included here model predictions that best fit a maximum number of observable parameters. Observational data are given in the second line of the corresponding entries. Note that the observational  $W(H\beta)$  and  $L(WR)/L(H\beta)$  values have been corrected as explained in the text. The  $L(4860)_{sb}/L(4860)_{tot}$  ratio measures the fraction of the continuum at 4860 Å originated by the young stars over the total continuum within the aperture, as explained in the text. When both Extended and Instantaneous Burst models could be fitted, the best fitting one has been considered, and the age derived from the second one has been included within parentheses.

	NGC 588	NGC 595	NGC 2363	IZw 18	Mrk 710	Tol 3	NGC 3256	Haro 2	Mrk 36
Metallicity ( $Z$ )	0.004	0.008	0.001	0.001	0.020	0.004	0.020	0.008	0.001
IMF slope	-1	-2.35	-2.35	-2.35	-2.35	-2.35	-3	-1	
Age (Myr)	2.8	3.1	2.6	13(3.0)	10(4.0)	3.0	4.5	4.8	2.9
SFR	IB	IB	IB	EB(IB)	EB(IB)	IB	IB	IB	IB
$E(B - V)_{UV}$	0.11	0.29	0.08	0.05	0.19	0.16	0.16	0.12	0.05
Extinction law	LMC	Gal	LMC	Gal	LMC	LMC	SMC	LMC	SMC
$E(B - V)_{opt}$	0.10	0.33	0.16	0.05	0.29	0.17	0.85	0.22	0.0
$L_{UV}^{synt}$ ( $\text{erg s}^{-1} \text{Å}^{-1} \text{M}_{\odot}^{-1}$ )	$1.81 \cdot 10^{33}$	$1.91 \cdot 10^{32}$	$4.14 \cdot 10^{32}$	$2.78 \cdot 10^{32}$	$1.39 \cdot 10^{32}$	$3.75 \cdot 10^{32}$	$1.22 \cdot 10^{32}$	$9.90 \cdot 10^{31}$	$7.38 \cdot 10^{33}$
$M_{trans}$ ( $\text{M}_{\odot}$ )	$5.34 \cdot 10^2$	$5.01 \cdot 10^3$	$4.69 \cdot 10^4$	$1.33 \cdot 10^5$	$1.42 \cdot 10^6$	$5.92 \cdot 10^5$	$9.84 \cdot 10^7$	$6.62 \cdot 10^6$	$9.23 \cdot 10^3$
$L(4860)_{sb}/L(4860)_{tot}$	–	–	1.0	0.5	0.4	0.5	0.6	0.6	–
$W(\text{Si IV})/W(\text{C IV})$	0.2	0.5	0.3	–	0.6	0.4	1.0	1.0	0.2
	0.14	0.54	–	–	0.71	0.45	1.0	0.98	0.20
$W(H\beta)$ (Å)	100	91	300	137	100	90	33	45	115
	97	100	300	135	90	85	40	50	110
$T_{eff}$ (K)	39000	37300	42000	42000	40300	38900	33800	34500	41000
	36600	35000	42700	35000	39800	38200	37000	35400	40000
$L(WR)/L(H\beta)$	0.0	0.05	0.0	0.0005	0.04	0.05	0.20	0.04	0.0
	–	–	0.0	0.05	0.06	0.09	–	0.06	–
$L(H\beta)$ ( $\text{erg s}^{-1}$ )	$5.1 \cdot 10^{37}$	$1.1 \cdot 10^{38}$	$1.9 \cdot 10^{39}$	$1.9 \cdot 10^{39}$	$1.6 \cdot 10^{40}$	$1.5 \cdot 10^{40}$	$2.2 \cdot 10^{41}$	$1.8 \cdot 10^{40}$	$9.4 \cdot 10^{38}$
	$1.2 \cdot 10^{38}$	$4.5 \cdot 10^{38}$	$1.6 \cdot 10^{39}$	$1.5 \cdot 10^{39}$	$1.8 \cdot 10^{40}$	$1.6 \cdot 10^{40}$	$1.9 \cdot 10^{42}$	$4.2 \cdot 10^{40}$	$7.3 \cdot 10^{38}$
$L_{FIR}$ ( $\text{erg s}^{-1}$ )	$1.4 \cdot 10^{40}$	$4.5 \cdot 10^{40}$	$2.8 \cdot 10^{41}$	$2.6 \cdot 10^{41}$	$5.5 \cdot 10^{42}$	$4.7 \cdot 10^{42}$	$1.5 \cdot 10^{44}$	$8.9 \cdot 10^{42}$	$2.0 \cdot 10^{41}$
	$\leq 1.2 \cdot 10^{40}$	$\leq 8.3 \cdot 10^{40}$	$2.7 \cdot 10^{41}$	$< 2.6 \cdot 10^{41}$	$7.4 \cdot 10^{42}$	$5.3 \cdot 10^{42}$	$1.9 \cdot 10^{45}$	$1.6 \cdot 10^{43}$	$\leq 1.4 \cdot 10^{41}$
$L_{radio}$ ( $\text{Jy kpc}^2$ )	$1.5 \cdot 10^4$	$3.5 \cdot 10^4$	$5.6 \cdot 10^5$	$4.9 \cdot 10^5$	$5.4 \cdot 10^6$	$4.5 \cdot 10^6$	$1.1 \cdot 10^8$	$6.3 \cdot 10^6$	$2.8 \cdot 10^5$
	–	$6.3 \cdot 10^4$	$1.3 \cdot 10^6$	$2.3 \cdot 10^6$	$6.0 \cdot 10^8$	$5.9 \cdot 10^6$	$1.3 \cdot 10^9$	$6.1 \cdot 10^7$	$1.5 \cdot 10^6$
$\alpha_{radio}$	-0.1	-0.2	-0.1	-0.2	-0.2	-0.1	-0.2	-0.3	-0.1
	–	$\approx 0$	$\approx 0$	-0.12	-0.8	–	–	-0.86	–

It has been postulated in the past that strong ionizing flux produced by newly formed massive stars could inhibit further formation of stars, explaining why massive stars seem to be coeval in many bursts. On the other hand, we have found that massive stars have been continuously formed during several million years in some galaxies. HST imaging of IZw 18, for example, has allowed to identify individual clusters with different ages (Hunter & Thronson 1995). The superposition of several of these clusters at different ages would mimic an extended star formation episode when analyzed globally. Therefore, the detection of starbursts forming stars during extended periods of time can still be reconciled with the idea that individual clusters of massive stars are coeval.

The spread in the evolutionary status of the studied starbursts is rather narrow. Their mean age is around 4 Myrs, in any case within the range 2.5-6.5 Myrs. Our sample is obviously biased toward very young bursts, since galaxies have been selected from their strong emission lines. After some 7 Myrs of an instantaneous burst the ionizing flux decreases significantly, so that no strong emission lines would be expected. Older starbursts, at ages above 7 Myr, should be detected from their powerful FIR emission and large amounts of red supergiant stars. We have shown indeed in Mas-Hesse & Kunth (1991a) that the FIR luminosity decreases with time much slower than the ionizing emission, since it originates mainly from the absorption of UV photons longward of the Lyman limit. This seems to be the case of many IRAS galaxies with very weak or absent



**Table 7.** *Continuation.*

	NGC 4214	I Zw 36	NGC 4670	Mrk 59	NGC 5253	NGC 5471	I Zw 70	IC 4662
Metallicity ( $Z$ )	0.008	0.001	0.008	0.004	0.004	0.004	0.004	0.004
IMF slope	-2.35	-2.35	-3	-3	-3	-2.35	-1	-3
Age (Myr)	3.5	2.7	4.0	3.0	3.0	2.9	3.8	13(4.0)
SFR	IB	IB	IB	IB	IB	IB	IB	EB(IB)
$E(B - V)_{UV}$	0.07	0.007	0.13	0.05	0.10	0.07	0.09	0.047
Extinction law	SMC	SMC	LMC	Gal	SMC	Gal	LMC	SMC
$E(B - V)_{opt}$	0.28	0.0	0.32	0.0	0.19	0.15	0.17	0.09
$L_{UV}^{synt}$ ( $\text{erg s}^{-1} \text{ \AA}^{-1} \text{ M}_{\odot}^{-1}$ )	$5.06 \cdot 10^{32}$	$2.14 \cdot 10^{33}$	$1.11 \cdot 10^{32}$	$1.90 \cdot 10^{32}$	$1.40 \cdot 10^{32}$	$5.83 \cdot 10^{32}$	$1.26 \cdot 10^{33}$	$1.19 \cdot 10^{32}$
$M_{trans}$ ( $\text{M}_{\odot}$ )	$2.63 \cdot 10^5$	$1.28 \cdot 10^4$	$3.03 \cdot 10^6$	$1.49 \cdot 10^6$	$8.00 \cdot 10^5$	$1.17 \cdot 10^5$	$2.17 \cdot 10^5$	$5.35 \cdot 10^5$
$L(4860)_{sb}/L(4860)_{tot}$	0.5	1.0	0.5	1.0	0.5	–	0.8	–
$W(\text{Si IV})/W(\text{C IV})$	0.5	0.2	0.8	0.6	0.6	0.4	0.3	0.0
	0.67	–	0.82	0.91	0.59	0.50	0.30	1.0
$W(H\beta)$ ( $\text{\AA}$ )	80	300	61	128	140	115	45	64
	90	300	54	135	160	129	60	65
$T_{eff}$ (K)	36700	41000	36000	38500	39000	39000	36800	40000
	37000	40000	37000	40000	37000	39000	36000	38000
$L(WR)/L(H\beta)$	0.05	0.0	0.06	0.003	0.003	0.005	0.11	0.003
	0.05	–	$\leq 0.1$	0.08	0.009	0.02	–	0.005
$L(H\beta)$ ( $\text{erg s}^{-1}$ )	$4.1 \cdot 10^{39}$	$5.1 \cdot 10^{38}$	$1.2 \cdot 10^{40}$	$1.2 \cdot 10^{40}$	$7.0 \cdot 10^{39}$	$3.2 \cdot 10^{39}$	$6.8 \cdot 10^{39}$	$1.9 \cdot 10^{39}$
	$1.3 \cdot 10^{40}$	$8.6 \cdot 10^{38}$	$2.1 \cdot 10^{40}$	$1.4 \cdot 10^{40}$	$6.9 \cdot 10^{39}$	$2.0 \cdot 10^{39}$	$1.4 \cdot 10^{40}$	$2.2 \cdot 10^{39}$
$L_{FIR}$ ( $\text{erg s}^{-1}$ )	$1.2 \cdot 10^{42}$	$3.7 \cdot 10^{40}$	$5.3 \cdot 10^{42}$	$2.0 \cdot 10^{42}$	$1.6 \cdot 10^{42}$	$6.0 \cdot 10^{41}$	$2.6 \cdot 10^{42}$	$4.3 \cdot 10^{41}$
	$5.3 \cdot 10^{42}$	$< 9.4 \cdot 10^{40}$	$3.1 \cdot 10^{42}$	$2.0 \cdot 10^{42}$	$4.0 \cdot 10^{42}$	$6.0 \cdot 10^{41}$	$2.1 \cdot 10^{42}$	$1.1 \cdot 10^{42}$
$L_{radio}$ ( $\text{Jy kpc}^2$ )	$1.4 \cdot 10^6$	$4.7 \cdot 10^5$	$4.2 \cdot 10^6$	$3.5 \cdot 10^6$	$2.0 \cdot 10^6$	$9.6 \cdot 10^5$	$2.8 \cdot 10^6$	$6.5 \cdot 10^5$
	$3.6 \cdot 10^7$	$2.5 \cdot 10^6$	$1.5 \cdot 10^7$	$4.8 \cdot 10^6$	$1.0 \cdot 10^7$	$4.0 \cdot 10^6$	$1.3 \cdot 10^6$	–
$\alpha_{radio}$	-0.2	-0.1	-0.3	-0.1	-0.1	-0.1	-0.4	-0.2
	-0.4	$\geq -0.3$	–	-0.6	-0.1	-0.2	-0.3	–

emission lines. NGC 4945 is a good example of a galaxy in this post-burst phase. Koornneef (1993) has shown that mass loss from massive red stars and supernovae from red supergiants progenitors dominate its energetics, and has proposed the name Post-burst Infrared Galaxy for objects in this particular evolutionary stage. We would expect a relatively high number of supernova explosions in these galaxies hence with non-thermal radio emission and spectral indices close to -1.0. Note that an extended star formation process could not produce in any case such a high FIR output together with the weak emission lines found in these galaxies, since ionizing photons would be produced continuously at a very high rate.

Derived ages are in any case model dependent. The parameterization of  $W(H\beta)$  as a function of time strongly depends on the number of ionizing photons predicted by stellar atmosphere models as well as on the assumed number of photons directly absorbed by dust. Moreover, if the IMF upper mass limit is below  $120 \text{ M}_{\odot}$  the age determination would become rather imprecise during the first million years, as shown by Leitherer &

Heckman (1995) for starbursts with upper mass limits of only  $30 \text{ M}_{\odot}$ . Therefore more than the absolute ages we can derive the evolutionary state of the different objects inter-compared with each others.

Our models however are weakly sensitive to previous episodes of star formation but rather to the most massive stars formed, hence the ones younger than 10 Myr. Previous bursts of star formation would not be detected by our method. Nevertheless, the remnants of such bursts would still provide a significant contribution to the optical continuum. We believe that this is the case in the few galaxies in which a significant excess of optical emission has been detected (NGC 4670, Mrk 710, Haro 2, NGC 4214, Tol 3 and I Zw 70). However the fact that in the majority of these galaxies the observed  $WR/(WR + O)$  ratio is rather large rejects the possibility that massive star formation has proceeded at a continuous rate during such a large period of time.

### 5.2. Initial Mass Function

To isolate the effects of the IMF slope we have to select observational parameters weakly affected by extinction and well behaved with respect to age (i.e., monotonous functions of time). Ideal parameters are line equivalent widths, like  $W(H\beta)$  and  $W(\text{Si IV})$  and  $W(\text{C IV})$ .  $W(H\beta)$  decreases almost continuously with time and is weakly dependent on the IMF slope (Mas-Hesse & Kunth 1991a). On the other hand, the  $W(\text{Si IV})/W(\text{C IV})$  ratio increases with time and depends on the IMF slope, since it is a good tracer of the relative number of O3-O8 stars versus B0-B3 ones (see Fig. 1 of Mas-Hesse & Kunth 1991a). Therefore, combining both parameters it should be possible to constrain simultaneously the age and the IMF slope, as we have shown in previous sections. Note that we are only considering the upper section of the IMF ( $M > 10 M_{\odot}$ ), since our method is insensitive to the relative amount of low mass stars (see Mas-Hesse & Kunth 1991a for a discussion on the effects of low mass stars).

We find that the IMF slope is constrained to the narrow range 1 to 3, with a mean value between Salpeter one ( $\alpha = 2.35$ ), and Scalo (1986) ( $\alpha = 2.85$  for the upper section of the IMF). Despite some scatter in the derived values of the IMF slope, as shown in Figs. 4, we find no correlation between the precise value of the slope and other properties of the star formation episodes. We report however that objects showing flatter IMFs are always small, compact star-forming regions, like NGC 588, Mrk 36 and IIZw 70. On the other hand, four of the galaxies (NGC 4214, NGC 4670, NGC 5253 and Haro 2) with optical continuum more clearly dominated by a previous generation of stars show rather steep IMFs with  $\alpha$  values close to 3. The previous bursts of star formation known to have taken place in these galaxies could have modified the properties of the interstellar clouds hampering the formation of lower mass stars. It is interesting to note that apart  $W(H\beta)$  and  $W(\text{Si IV})/W(\text{C IV})$ , the rest of the parameters could have been rather well fitted assuming a standard value of the IMF slope (see for instance Rosa & Benvenuti 1994).

Another important result from this work is that we find no correlation between the metallicity and the slope of the IMF. The trend toward flatter IMFs at low metallicities proposed in the past (Melnick et al. 1985; Viallefond 1986) is therefore not confirmed by our results. This trend was proposed to explain the apparent correlation toward higher values of the effective temperature and  $W(H\beta)$  values at low metallicities. Cerviño & Mas-Hesse (1994) showed that the effects on the evolution of massive stars of decreasing the metallicity could account for this observational trend. We have plotted in Fig. 9 the predicted  $W(H\beta)$  and effective temperature vs. the O/H abundance at different evolutionary stages of the cluster, assuming nearly instantaneous star formation episodes. This figure shows a clear trend toward higher  $W(H\beta)$  and  $T_{eff}$  values the lower the metallicity, even with identical IMFs. We can see that at 2.75 Myr (just before the first WR stars have been produced),  $W(H\beta)$  is higher at  $Z = Z_{\odot}/20$  than at  $Z = 2Z_{\odot}$  by almost an order of magnitude. This effect is even stronger at older ages.

$W(H\beta)$  values predicted by evolutionary synthesis models during the first 2 Myr can be as high as  $\sim 500 \text{ \AA}$ , with a fast decrease afterwards. Nevertheless, the observational values of  $W(H\beta)$  seldom exceed  $350 \text{ \AA}$  (see for example the catalogue of H II galaxies by Terlevich et al. 1991). If the IMF is complete up to around  $120 M_{\odot}$ , this lack of high  $W(H\beta)$  objects would indicate that almost no starburst younger than 2 Myr has been observed. By an obvious statistical effect, we would expect to find emission-line galaxies covering more or less uniformly the age range between 0 and 6 Myr (when the emission lines fade), so that this discrepancy reflects a weak point of evolutionary synthesis models. This effect can not be attributed to flatter than normal IMFs, since the IMF slopes in these regions are similar to that of the solar neighborhood. The possible contamination of the optical continuum by an underlying stellar population can neither account for this effect. We have seen that the emission associated to the present burst generally dominates even at optical wavelengths and that the underlying continuum is generally negligible. Moreover, we have been able to correct  $W(H\beta)$  from the contamination by underlying stars. The discrepancy could be minimized if the upper mass limit is lowered to around  $60 M_{\odot}$ . In such a case the maximum values of  $W(H\beta)$  would remain below around  $350 \text{ \AA}$  at any time, in accordance with observational results (Mas-Hesse & Kunth 1991a). Nevertheless, stars with initial masses in the range  $80\text{-}100 M_{\odot}$  (but not larger!) have been found in the Magellanic Clouds (Massey et al. 1995; Heydari-Malayeri 1996), so that there are no good reasons to truncate the IMF at around  $60 M_{\odot}$  (Scalo 1986, 1990). Bernasconi & Maeder (1996) have proposed recently that, since accretion leading to the formation of massive stars should take around 2–2.5 Myr, stars with initial masses above  $40 M_{\odot}$  would emerge from its parental cloud with a substantial fraction of its central hydrogen content already burned. As a result, the formal Main Sequence lifetime would be reduced and, at the time the star becomes visible, it would have already evolved to lower effective temperatures. We postulate that this effect could be at the origin of this discrepancy, explaining why no starbursts younger than 2 Myr have been identified. Nevertheless, to confirm this hypothesis new models have to be built taken into account the accretion time of the most massive stars.

Another possible explanation of this discrepancy could be an overestimation of the Lyman continuum photons predicted by the models. First, the fraction of photons that do not contribute to the ionisation process could have been underestimated. We have assumed through this work that a fixed fraction of 30% of the photons are directly absorbed by dust. This value corresponds to the average fraction in Galactic H II regions, as we have discussed above. Nevertheless, the compilation by Smith et al. (1978) shows that this parameter covers a range between 80% and 20% in our Galaxy. It is difficult to extrapolate which should be the correct value when analyzing the integrated emission from large star-forming regions in external galaxies, but we want to note that changing the average fraction to 60%, instead of 30%, would reconcile the observations with the model predictions. A second possibility would

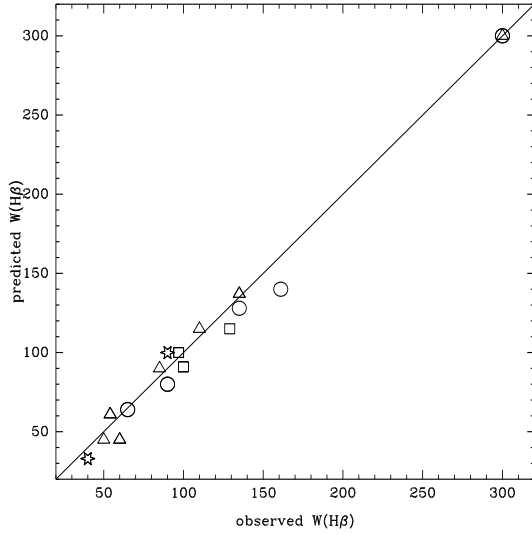


**Fig. 6.** Predicted vs. observed  $W(H\beta)$  values in Å. Squares: GH II regions; circles: irregulars; triangles: blue compacts; stars: spiral and merger.

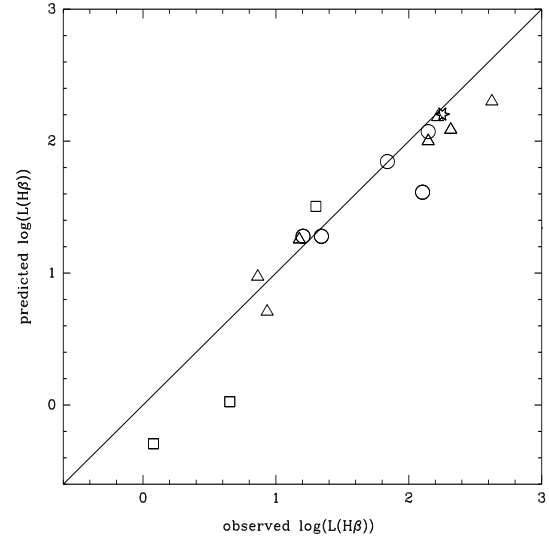


**Fig. 8.** Predicted vs. observed  $L(H\beta)$  values in units of  $10^{38}$  erg/s. Symbols as in Fig. 6.

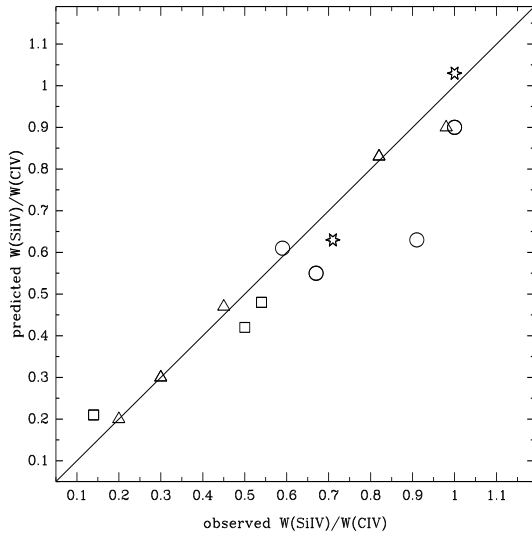


**Fig. 7.** Predicted vs. observed  $W(\text{Si IV})/W(\text{C IV})$  values. Symbols as in Fig. 6.

be the presence of systematic errors in stellar atmosphere models. As discussed by Scalo (1990) different computations can show a spread of up to an order of magnitude in the number of ionizing photons emitted even at masses as small as  $30 M_{\odot}$ . Nevertheless, Schaerer et al. (1995) have analyzed the effects of combining stellar structure and atmosphere models on the ionizing flux, treating consistently the entire mass loss from the center out to the stellar winds. They find that while the shape of the ionizing continuum can be strongly modified with respect to plane-parallel models, the total number of ionizing photons is not significantly modified.

If massive stars formation proceeds as episodic instantaneous bursts, the formation of low mass stars could be seriously hampered. The time needed for the protostellar collapse of a low mass cloud is at least several million years, in any case longer than the time required for the formation of the most massive stars. Therefore, if we assume that the onset of massive stars inhibits further star formation, low mass could be very deficient in these regions. Nevertheless, Zinnecker et al. (1996) have found from X-ray and IR imaging that OB associations contain stars with masses below  $1 M_{\odot}$ , and that 30 Dor-like associations may be surrounded by low mass stars. Low mass stars seem therefore to have formed prior to the massive stars, as postulated by Tenorio-Tagle (1994). Under this scenario the whole population of low mass stars would form at the very beginning of the collapse. Shocks induced in the gas by the movement of these stars would trigger the collapse of more massive stars. These massive stars would finally heat the gas, inhibiting further star formation. In this way, the whole IMF would be filled with stars.

### 5.3. Wolf-Rayet stars population

We have plotted in Figs. 10a,b the predicted  $L(WR)/L(H\beta)$  ratios and  $W(WR_{bump})$  for different metallicities, two limiting values of the IMF slope and both star formation regimes. We have included in Figs. 10a,b the mean values of the  $L(WR)/L(H\beta)$  ratios and  $W(WR_{bump})$  of a more complete sample of galaxies compiled from Kunth & Joubert (1985), Kunth & Schild (1986) and Vacca & Conti (1992) (see also the comparisons made by Maeder & Meynet 1994 and Meynet 1995). Points have been located at their mean ages, as estimated by the  $W(H\beta)$  values. Error bars indicate the range of ages covered. Nevertheless, these age estimates are only ap-

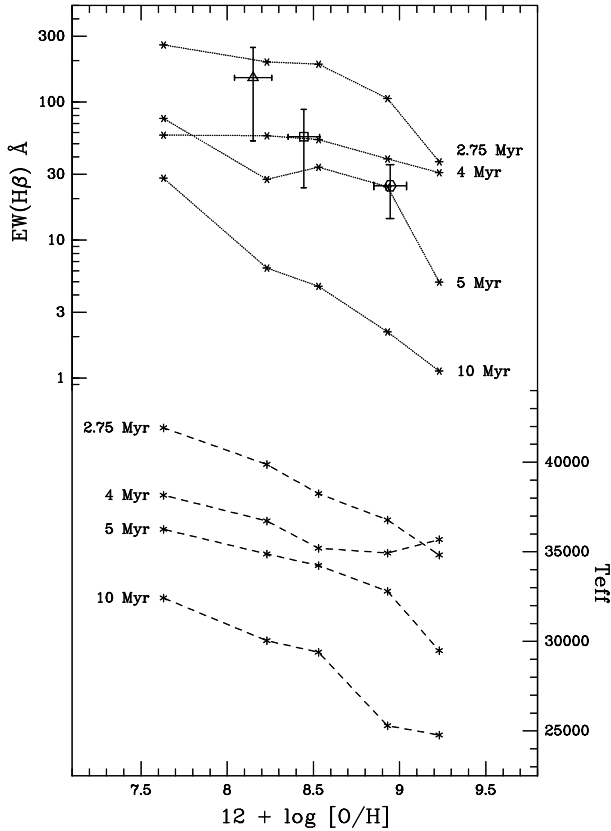
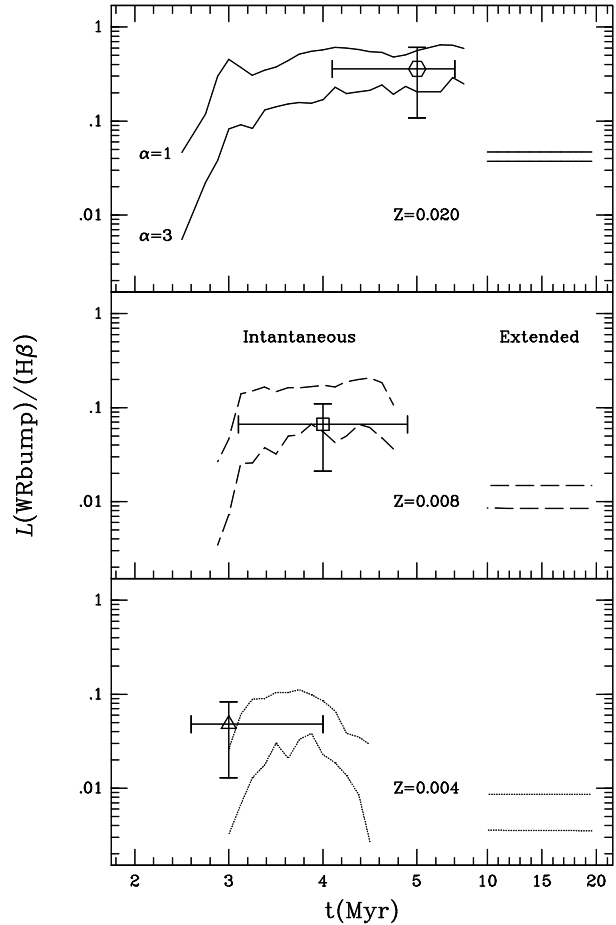


**Fig. 9.** Predicted  $W(H\beta)$  and  $T_{eff}$  as a function of metallicity for different ages. There is a clear tendency to smaller values of both parameters the higher the metallicity.

proximate, since no correction at all has been applied to the observational values, generally taken through narrow slits.

It can be seen that our results can be extended to this more complete sample. The average  $W(H\beta)$  and  $W(WR_{bump})$  values fall fairly well within the limiting predicted curves. It is also remarkable that the derived range of ages coincide rather well with the ages at which WR stars are expected. Although the lower limits of the error bars would be in some few cases compatible with extended star formation regimes, the average ratios suggest again that the star formation episodes should have taken place almost instantaneously. The fact that also in this more extended sample the agreement with the  $W(WR_{bump})$  values is satisfactory indicates that in these galaxies the burst emission largely dominates in general over the older underlying stellar population.

Schaerer (1996) has evaluated the effect of the evolution of the WR stars population on the He II narrow emission line at 4686 Å, by combining model atmospheres accounting for stellar winds with evolutionary tracks. He concludes that for metallicities in the range  $Z = Z_{\odot}/5 - Z_{\odot}$  a strong nebular He II emission line should originate in early WR phases when WC stars begin to appear. The He II emission line is indeed detected in few objects with very young ages, below 3 Myr, and there-

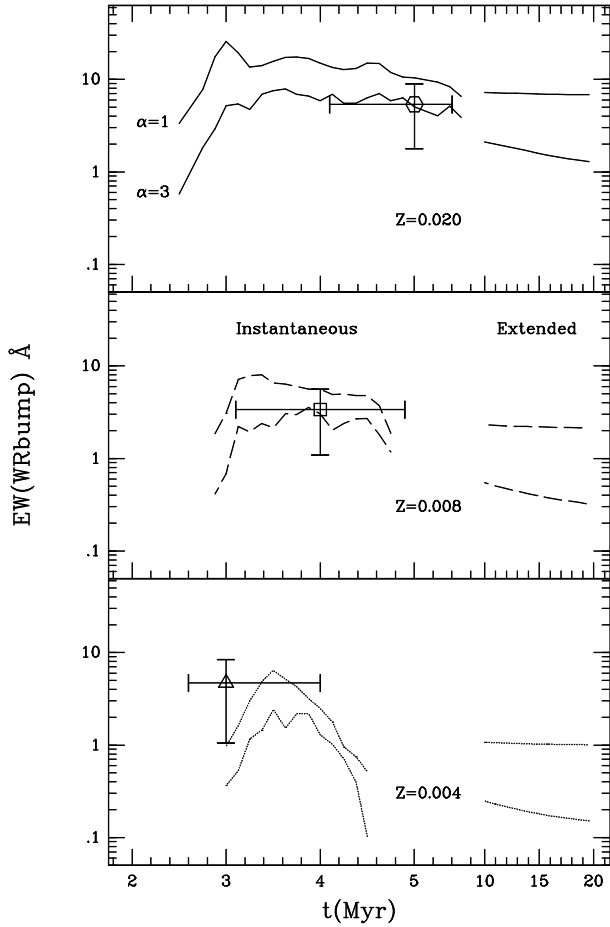


**Fig. 10.** a)  $L(WR)/L(H\beta)$  ratio and b)  $W(WR_{bump})$  predicted by the models. We have plotted here the predictions for the limiting values of the IMF slope considered and for both instantaneous and extended star formation regimes, this latter one only for ages above 10 Myr. Mean values from an extended sample of objects (see text) have been included. Note that they are generally located within the predicted bands.

fore starting to produce WR stars (NGC 2363 and Mrk 36), in good agreement with the scenario proposed by Schaerer.

#### 5.4. Supernovae and radio emission

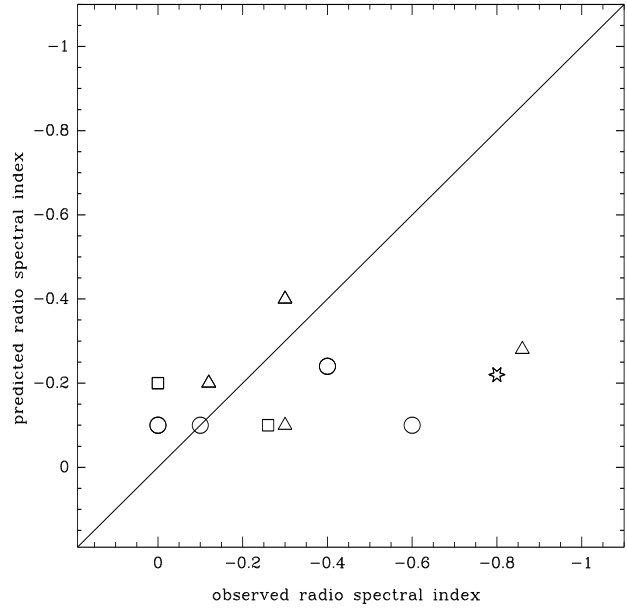
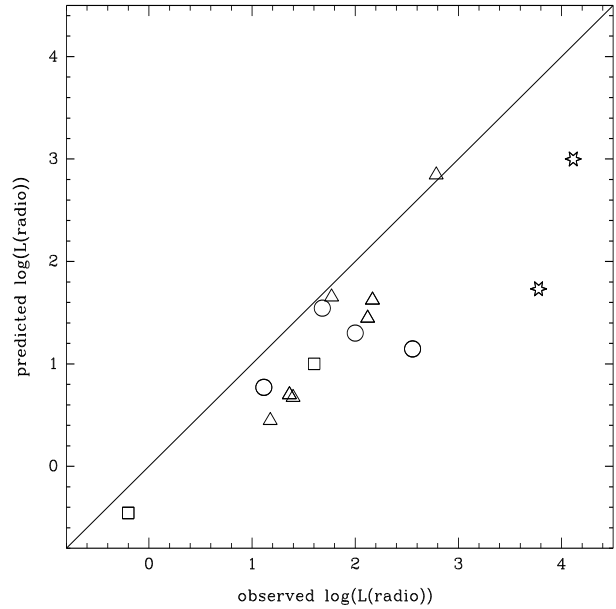
The relatively large number of massive stars in these small regions originate frequent supernova explosions after the first 3 Myr, when the most massive stars (initial mass around  $120 M_{\odot}$ ) end their lifetime. The evolution of the supernova rate depends strongly on the IMF slope, as discussed in Cerviño & Mas-Hesse (1994). For slopes between  $\alpha = 2$  and 3 the supernova rate varies only weakly with time. Around  $10^{-9} \text{ yr}^{-1} M_{\odot}^{-1}$  supernovae explosions are expected with an increasing supernovae rate the higher the metallicity. Considering the mass involved in the star-forming episodes, we expect supernova rates in the range  $10^{-7}$  (NGC 588) to  $10^{-3} \text{ yr}^{-1}$  (Haro 2). Typical values for compact galaxies are around 1 su-


**Fig. 10.** Continuation

pernova each 1000 years and remains almost constant after the first 3 Myr, up to around 50 Myr, when stars of initial mass around  $6 M_{\odot}$  end their lifetime. Therefore, thousands of supernova explosions must have taken place within the relatively small star-forming regions of the most evolved objects we have studied.

The large number of supernova remnants (SNR) must become strong sources of non-thermal radio emission. Depending on the evolutionary state of the star formation episode the total radio emission should be dominated by nebular thermal free-free emission, with a flat radio spectral index ( $\alpha_{radio} \sim -0.1$ ) or by the non-thermal contribution from SNR ( $\alpha_{radio} \sim -0.9$ ) (see Mas-Hesse 1992 for a more detailed discussion of radio emission from starbursts).

We have plotted in Figs. 11 and 12 the predicted vs. the observed radio spectral indices and radio luminosities at 6 cm, respectively. It is clear that our models significantly underestimate the observed radio luminosities. The predicted emission is underestimated by factors between 2 (NGC 595, NGC 2363 and Mrk 59) and around 5 for the majority of BCGs (IZw 18, Mrk 36, IZw 36, NGC 4670, NGC 5471 and IIZw70). In all these objects the thermal contribution is dominating, since they are younger than 4 Myr and have had no time for a significant


**Fig. 11.** Predicted vs. observed radio spectral indices around 6 cm. Symbols as in Fig. 6.

**Fig. 12.** Predicted vs. observed radio luminosities at 6 cm in units of  $10^5 \text{ Jy kpc}^2$ . Symbols as in Fig. 6.

number of supernova explosions. The radio spectral indices are indeed above  $\alpha_{radio} = -0.3$  (except for Mrk 59), as predicted by the models. The radio emission in IZw 18, an object having experienced a sequence of bursts during the last 13 Myrs, is also purely thermal, showing that the contribution of non-thermal sources becomes negligible when a large number of ionizing stars are present.

The thermal radio emission is a known function of the number of ionizing photons emitted. Since our models are matched

to reproduce the intensity of the Balmer lines, which are also a linear function of the number of ionizing photons, there should be a good agreement between the observed and predicted thermal radio emissions, but this is not the case. The discrepancy between the observed Balmer lines emission and the thermal radio luminosity is a well-known problem (Israel & Kennicutt 1980; Lequeux et al. 1981; Caplan & Deharveng 1986; Skillman & Israel 1988). The most accepted explanation is that the effective reddening in the radio range is smaller than in the optical, due essentially to geometrical effects and a patchy distribution of dust. Nevertheless, since the massive stellar population we derive reproduces well the de-reddened Balmer line fluxes (within less than a factor 1.6 in average), the intrinsic total number of ionizing photons injected to the nebular gas should be well constrained. A possible explanation for this discrepancy would be the presence of a large number of ionizing stars in small regions completely obscured by dust in the optical, from which only the associated radio emission could escape (and partially also the near infrared emission lines). This scenario is nevertheless not consistent with our results, since the large number of hidden stars we would need to reproduce the observed radio emission would increase significantly the observed FIR luminosities contrary to what we observe (see next section). Inhomogeneous scattering, depending on the specific geometrical distribution of dust in each galaxy and with different efficiencies at radio and optical ranges, might provide the additional contribution to the observed radio emission (Caplan & Deharveng, 1986). If this explanation is valid, a word of caution should be given against deriving intrinsic extinctions from the observed ratio between radio and Balmer lines emission, since the reddening can be significantly overestimated.

For larger galaxies the underestimation of the radio emission is even more severe, between a factor 10 for Haro 2 and two orders of magnitude for Mrk 710. These discrepancies can be partly attributed to aperture mismatch, especially important in these large galaxies, as well as to the expected contribution of supernova remnants from previous episodes of star formation. As we have discussed above, supernovae events can be active until more than 50 Myr, when the stellar contribution to the UV continuum and to the ionisation process has become negligible. In this sense it is interesting to note that the three galaxies for which the discrepancy is larger (Haro 2, NGC 4214 and Mrk 710) show radio spectral indices below  $\alpha_{radio} = -0.4$ , i.e. dominated by non-thermal sources.

### 5.5. Far Infrared Emission

The Far Infrared emission in objects dominated by intense star formation episodes is essentially due to thermal emission by dust particles heated by the UV stellar radiation field. This process of absorbing high energy photons, re-emitted at low energies (typically at around  $100 \mu\text{m}$ ), can be so efficient that the FIR luminosity becomes a good approximation to the bolometric luminosity. Since the origin of this FIR emission is mainly the energy output of massive stars, whose UV photons are efficiently absorbed by dust,  $L_{FIR}$  has been used in the past to

derive the number of massive stars in the young clusters, and henceforth the star formation rate (Hunter et al. 1986).

The technique we have used to fit the unreddened synthetic SEDs to the actually observed ones provides a direct estimation of the expected total FIR luminosity. As we have explained in detail in Mas-Hesse & Kunth (1991a) we compute the total energy absorbed by dust from the difference between the unreddened synthetic SED and the reddened SED that best fits the observed spectrum. We take into account the energy provided by Lyman  $\alpha$  photons which are absorbed by dust and a fixed fraction of 30% of the Lyman continuum photons which are absorbed by dust and do not contribute to ionisation.

Calzetti et al. (1995) have estimated the expected contribution to the FIR emission of a large sample of star-forming galaxies by assuming a single extinction law (Calzetti et al. 1994) and a color excess derived from the Balmer decrement, decreased by 0.5 mag. While this approach might be useful to derive average properties of a large sample, our procedure derives first both the shape and the strength of the extinction law affecting the continuum, and uses these results to compute the expected FIR luminosities. These authors separate the FIR emission coming from cool ( $T_{dust}$  around 20 K) and warm ( $T_{dust}$  around 40 K) dust, as also proposed by Buat & Deharveng (1988). In our sample star formation processes are so intense that the FIR emission is dominated by the warm dust. The mean dust temperature is around 40 K, as shown in Table 5, so that a two-components deconvolution is not needed. Furthermore, the emission in the IRAS bands below  $60 \mu\text{m}$  is generally very low and has not been detected, so that the extrapolation to the whole FIR emission based on the 60 and  $100 \mu\text{m}$  fluxes can be taken as a good estimation of  $L_{FIR}$ .

We have plotted in Fig. 13 the predicted vs. observed FIR luminosities. It can be seen that both values are in general in good agreement.  $L_{FIR}$  is underestimated only in the case of spatially extended galaxies since while the predictions have been normalized to the energy emitted within the  $10'' \times 20''$  IUE aperture, IRAS fluxes were integrated over the whole galaxy. The discrepancy is highest for NGC 4214, in which there are known sites of massive star formation outside the IUE aperture (Maíz-Apellániz et al. 1998). As we have discussed in the previous section, the good agreement between predictions and observations, especially for spatially compact objects, indicates that we are sampling the whole population of massive stars, even at UV wavelengths (the measured UV continuum is used for de-normalization), and that the contribution from stars hidden within dust clouds is negligible. The only exceptions are NGC 595 and NGC 3256, a very dusty galaxy, in which only a small fraction of massive stars contribute to the UV continuum while the majority of the newly formed stars are apparently completely obscured by dust. Calzetti et al. (1995) have also found that an average of 30% of massive stars might be embedded in dusty regions within dusty galaxies, where  $E(B - V) > 0.25$ .

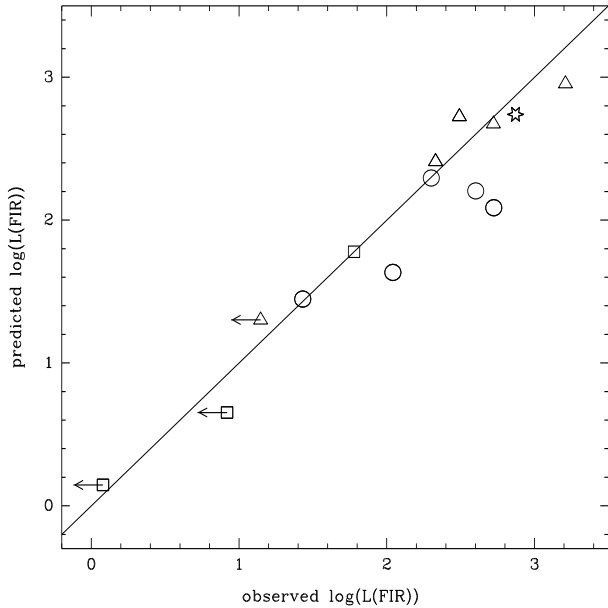


**Fig. 13.** Predicted vs. observed FIR luminosities in units of  $10^{40}$  erg/s. Symbols as in Fig. 6.

### 5.6. Extinction

Our sample is biased towards low reddening galaxies with strong UV continuum with the exception of NGC 3256, selected by its strong FIR emission and showing by far the strongest extinction. Nevertheless, as we have discussed above, even a small amount of dust can significantly modify the strength and shape of the UV continua.

From our analysis it becomes evident that the dust absorption feature at around  $2175 \text{ \AA}$  is very weak in these galaxies or even inexistent. Relatively weak absorption bumps in starburst spectra have already been noted by several authors (Blitz et al. 1981; Lequeux et al. 1981; Rosa et al. 1984; Kinney et al. 1993). The weakness of this absorption feature induced us to include both the LMC and SMC extinction laws in our fitting procedure. It is important to note that these laws have a rather different shape in the UV than the standard Galactic one, apart from a weaker (LMC) or inexistent (SMC) absorption feature. Therefore, even when only the 1200-1950 IUE range is available it is possible to discriminate which of the laws is applicable. The method we have followed is very sensitive to both the shape of the law and its strength, discriminating between different laws for color excesses above  $E(B - V) = 0.05$ , with  $E(B - V)$  being determined at a precision of  $\delta(E(B - V)) = 0.02$ . An example is shown in Fig. 14, where we have plotted the best fit obtained assuming three different extinction laws.

In almost all cases interstellar extinction closely follows either an LMC or SMC-like law. Since there is a tendency to have weaker absorption features at  $2175 \text{ \AA}$  at lower metallicities in nearby galaxies (Galaxy - LMC - SMC) we would expect a similar trend in our sample. This is not the case since even near-

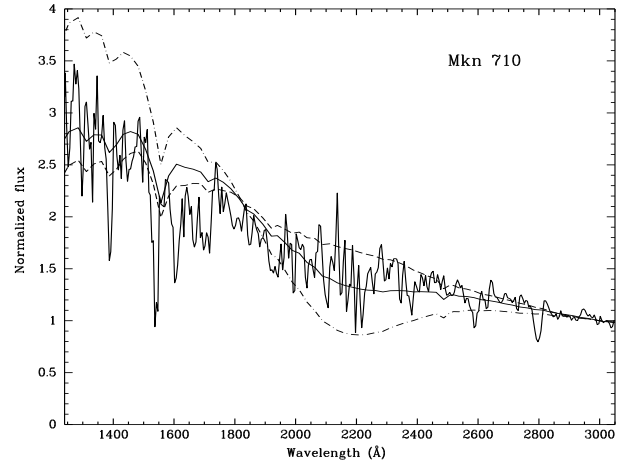


**Fig. 14.** Synthetic spectra reddened assuming three different extinction laws on top of the observed UV continuum of Mrk 710. Solid: best fitting law (LMC); dot-dashed: Galactic law; dashed: SMC law.

solar metallicity galaxies like Mrk 710 and NGC 3256 are best fitted assuming an LMC extinction law and not a Galactic one. The only object in our sample clearly affected by a Galactic-like extinction is NGC 595. Calzetti et al. (1994) have derived an universal UV to optical extinction law from the SED of 39 starburst and blue compact galaxies. This law and the Galactic one show similar optical-far UV slopes, but the Calzetti et al. (1994) one is essentially featureless. We stress here that the observed UV to optical SEDs can be very well reproduced by reddening the corresponding synthetic spectra with one of three extinction laws (Galactic, LMC and SMC) with no need to invoke an additional universal law.

The weakness of the absorption bump at  $2175 \text{ \AA}$  seems to be related to the intense star-formation processes taking place in these objects, rather than to the metallicity. The strong flux of high energy photons around the young massive clusters and the relatively high temperature that dust particles can reach in these environments affect most probably the size and composition of dust grains. Comparing the shape of the Galactic, LMC and SMC extinction laws with the absorption cross sections by amorphous silicates and graphite grains given by Mezger, Mathis & Panagia (1982) we conclude that graphite grains are deficient in starburst regions. An interstellar medium dominated by amorphous silicates would explain naturally both the weakness of the  $2175 \text{ \AA}$  bump and the steepness of the extinction law. Puget & Léger (1989) attribute the UV absorption bump to carbonaceous very small particles containing polycyclic aromatic molecules. They describe how a combination of photothermodissociation, double ionization and Coulomb explosion processes induced by an intense and hard UV radiation field would decrease significantly the abundance of these particles. We suspect that these processes do not depend on the metallicity of the environment, but on the intensity of the UV

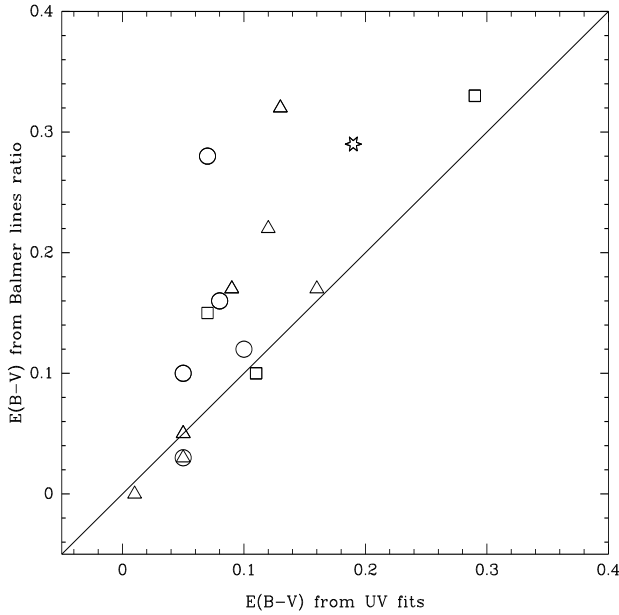


**Fig. 15.**  $E(B - V)$  values derived from Balmer lines ratios vs. values obtained from our UV continuum fitting procedure. Symbols as in Fig. 6 (NGC 3256 extreme case ( $E(B - V) = 0.85$  vs.  $0.16$ ) has not been included in the plot for scaling reasons).

emission, explaining the lack of correlation between the shape of the extinction law and the nebular metal abundance.

We have found that for several galaxies the  $E(B - V)$  values derived from the Balmer line ratios are systematically higher than values derived from the UV continuum (see Table 7). This discrepancy can be clearly appreciated in Fig. 15, where we have plotted both  $E(B - V)$  determinations. A similar effect has already been noticed by Fanelli et al. (1988), Keel (1993) and Calzetti et al. (1994) in the spectra of starburst galaxies.

It is important to remark that this UV-optical discrepancy is related to two very different sources of emission: stellar continuum and nebular emission lines. Two possible explanations for this discrepancy are the presence of strong absorption lines of stellar origin and geometrical effects. The usual correction for the contamination by stellar lines assumes absorption equivalent widths of around 1-2 Å and iterates until the color excesses derived from the  $H\alpha/H\beta$ ,  $H\beta/H\gamma$  and  $H\beta/H\delta$  ratios converge to the same value (McCall, Ribsky & Shields 1985). This is the method we have followed to derive the  $E(B - V)$  values, but it does not solve the discrepancy. On the other hand, from the synthesis of the Balmer lines absorption profiles, Díaz (1988) and Olofsson (1995) proposed that the stellar equivalent widths should be much larger, up to around 5 Å. We have therefore forced the  $E(B - V)$  value to be the same as obtained from UV continuum fits, and have derived so the corresponding equivalent widths of the absorption lines. In some cases the method converged, yielding consistent values of the absorption equivalent widths between 4 and 5 Å for the three Balmer lines

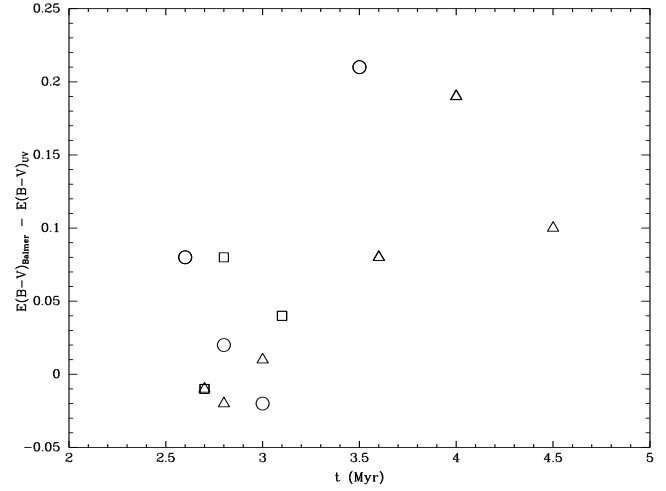


**Fig. 16.**  $E(B - V)$  values discrepancy as a function of derived age. Symbols as in Fig. 6.

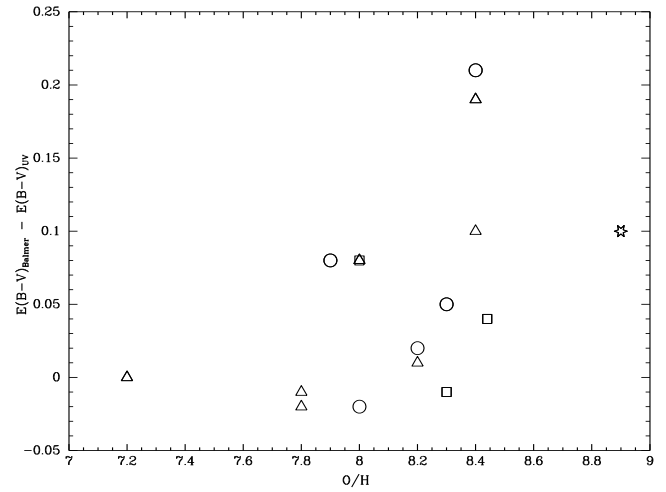


**Fig. 17.**  $E(B - V)$  values discrepancy as a function of nebular O/H abundance. Symbols as in Fig. 6.

$H\beta$ ,  $H\gamma$  and  $H\delta$ . But for the majority of the objects the equivalent widths did not match the relative strengths predicted by Díaz (1988).

The underlying stellar population seems to be responsible for this discrepancy in the case of Haro 2, at least partially. The method converged well, deriving stellar equivalent widths of 5.1, 4.2 and 4.1 Å for  $H\beta$ ,  $H\gamma$  and  $H\delta$ , respectively. Assuming this correction, the derived  $E(B - V)$  coincides with the value estimated from the UV continuum fits. Moreover, we have recently got high dispersion optical spectra of this galaxy and have been able to measure the equivalent widths of the stellar absorption lines (Legrand et al. 1997a), obtaining values in good agreement with the predicted correction ( $W(H\gamma) = 4.1 \pm 1.0$  Å;  $W(H\delta) = 4.7 \pm 1.0$  Å). We conclude that in some galaxies, the discrepancy between the strength of the extinction derived from the continuum and from the Balmer



decrement can be attributed to the presence of strong stellar absorption lines, associated to an underlying population of relatively low mass stars.

In NGC 4214, on the other hand, the required equivalent widths derived by this method varied between 13 and 6 Å for the different lines. Since such a large range of equivalent widths is not expected for the stellar absorption lines, we attribute the discrepancy to geometrical effects related to the inhomogeneous distribution of dust. While the continuum flux comes from the young clusters, the nebular emission originates in much more extended regions well beyond the ionizing sources. The strong ionizing flux is expected to affect the dust particles properties in the close surroundings of the massive stars. Stellar winds and supernova explosions might wipe out the dust from the neighbourhood of the massive clusters and concentrate it in filaments and dust patches still located within the ionized region. Depending on the specific geometrical distribution of dust and stars, the extinction could affect mainly the nebular gas emission but only weakly the stellar continuum.

In the specific case of NGC 4214, as we will discuss later, Maíz-Apellániz et al. (1998) have found that the Balmer line emission peaks at few arcseconds away from the massive stars cluster. Moreover, the reddening is highest in regions where Balmer lines are emitted while it is relatively low in front of the star cluster. The reddening in front of the cluster is consistent with that derived from continuum fits, while the reddening derived integrating spatially over the whole ionized region is significantly higher. These results have shown that an inhomogeneous distribution of dust can explain indeed the different extinctions derived from the stellar continua and the Balmer decrement. Nevertheless, this effect is not universal and depends strongly on the distribution of stars, gas and dust in each star-forming region. In the second brightest knot of star formation in NGC 4214 for example, the distributions of stars, ionized gas and dust are all centered in essentially the same regions. Our results are in good agreement with Gordon, Calzetti & Witt (1997), who also conclude from the analysis of the extinction in 30 starbursts that the stars/dust geometry should be close to a dust-free sphere of stars surrounded by an outer star-free shell of clumpy dust. We want to remark that since our method yields the extinction affecting the stellar continuum only, it might be well that the dust particles producing the UV bump have been destroyed from the neighbourhood of the massive stars, but they could still be present in the ionized gas located far away from the massive clusters.

We have found a trend toward higher  $E(B - V)_{Balmer} - E(B - V)_{UVcont}$  values the older the star-forming episode, as shown in Fig. 16. There is a well defined lower envelope, rising with age. On the other hand, note that the trend is very weak or even inexistent if we compare  $E(B - V)_{UVcont}$  with the age of the cluster (see Table 7). Similarly, although no clear trend with metallicity is found, the  $E(B - V)_{Balmer} - E(B - V)_{UVcont}$  discrepancy becomes highest for galaxies with O/H abundances above 8.4, i.e., objects whose interstellar medium has already been polluted by previous star formation episodes (see Fig. 17). We interpret these results as an evidence for an in-

terstellar medium enrichment with dust during the evolution of the clusters. This fraction of the extinction which is raising with time could be due to newly formed dust grains formed in stellar winds and in the supernova ejecta. In both cases dust would have been blown away from the stellar cluster, concentrating on given regions, still within the ionized nebula, but at a certain distance from the massive stars. In this way it would have a stronger effect on the emission lines than on the stellar continuum.

The discrepancy discussed hereabove has important implications on the analysis of starburst regions. First of all, the  $H\beta$  equivalent width, which is used as an age indicator can be affected by this differential reddening. A difference of  $\Delta(E(B - V)) = 0.2$  between nebular and continuum extinction implies an underestimation in the value of  $W(H\beta)$  by a factor of 2. Such discrepancies are not rare, as shown by Calzetti et al. (1995). They can lead to an overestimation of the age in some star-forming regions. A similar effect occurs when measuring the  $L(WR)/L(H\beta)$  ratio, since the WR bump originates in the atmosphere of these stars and should therefore be affected by the same extinction than the stellar continuum. Unfortunately, the only way to correct properly for this effect requires the mapping of the distribution of stars, gas and dust, something which is feasible only for nearby galaxies.

## 6. Analysis of some individual galaxies

We discuss in the next paragraphs the results we have derived for some representative individual objects.

### 6.1. NGC 5471

NGC 5471 is a massive GH II region located in M101. Our analysis yields a scenario characterized by a young (around 3.0 Myr), massive ( $1.2 \cdot 10^5 M_{\odot}$ ) cluster, following a standard IMF (slope slightly higher than the Salpeter value). Our age determination coincides with the value derived by Rosa & Benvenuti (1994) from HST FOS data, also based on the comparison with evolutionary synthesis models. NGC 5471 seems to be dominated by a well defined burst of star formation with a negligible contribution from older underlying stars. All the observational parameters can be reproduced by our models and only the radio emission is underestimated, as for the majority of the objects.

The effective temperature is high and hints toward the presence of stars more massive than at least  $40 M_{\odot}$ . Furthermore, the known existence of WR stars in this object of relatively low metallicity (O/H around 8.0) indicates that the IMF upper mass limit has to be very close to at least  $100 M_{\odot}$ , since only stars more massive than around  $80 M_{\odot}$  can become WR at this metallicity.

Reddening in NGC 5471 is moderate, with a derived color excess  $E(B - V) = 0.07$ . At this low reddening it becomes difficult to disentangle between the various extinction laws, but the Galactic one provides the best fit. This color excess derived from fitting the continuum is significantly smaller than

the value derived from the Balmer line ratio by Rosa & Benvenuti (1994),  $E(B - V) = 0.15$ . The good agreement between the predicted and the observed UV continua, as well as the FIR luminosities, let us conclude that the continuum cannot be reddened by more than  $E(B - V) = 0.07$ . This conclusion is reinforced by the good agreement of our 1200-7000 Å synthetic spectrum with the complete HST FOS spectrum of Rosa & Benvenuti (1994). As shown in Fig. 5, the fit is indeed rather good in the whole range, except for an overestimation of the continuum between 3700 and 4900 Å. The small region observed with FOS seems to be representative of the whole cluster, as observed through the large IUE aperture.

A broad  $H\alpha$  emission line ( $\text{FWHM} \approx 2000 \text{ km s}^{-1}$ ) was detected in this region by Castañeda et al. (1990) and was confirmed by Mas-Hesse et al. (1994). The origin of these broad line components is not yet well understood. One of the possible hypothesis relates such broad components with supernova activity. At the age derived for NGC 5471, close to 3 Myr, no supernovae should have yet taken place, since even stars with initial masses up to  $120 M_{\odot}$  need longer than 3.5 Myr to end their lives as supernovae. Therefore, our results provide a hint against this origin for the broad lines, and point rather to the effect of strong stellar winds, as proposed by Tenorio-Tagle et al. (1997) for other starbursts.

## 6.2. NGC 4214

NGC 4214 is a rather large irregular galaxy. It shows a central bar with several star-forming knots. The presence of incipient spiral arms led to its classification as SBmIII (Sandage & Bedke 1985). It has been scanned spectroscopically in the optical by Maíz-Apellániz et al. (1998), who have produced maps of the physical properties (extinction, density, excitation,...) and have also found line splitting and broad components at several locations. The overall view resulting from these observations is that several short lived star formation episodes have taken place over the bar connecting the two spiral arms of this galaxy, with a significant age spread (few Myr). Spectra and images of the brightest star-forming region have also been obtained with the Hubble Space Telescope by Leitherer et al. (1996), showing the presence of a bright, compact starburst knot surrounded by more than 200 fainter point-like sources. This compact region has been observed with IUE, including within its aperture a fainter knot located at  $8''$  to the East (Huchra et al. 1983).

Our best fitting models yield an age of around 3 - 3.5 Myr for this central star formation knot. The large number of WR stars detected indicates that this burst has been essentially instantaneous. Both the  $L(WR)/L(H\beta)$  ratio and the equivalent width of the WR bump constrain the age of the burst to between 3 and 5 Myr old. A broad WR feature attributed to  $C\text{ IV } \lambda 5808$  emission was detected in the two star-forming knots within the IUE aperture (Mas-Hesse & Kunth 1991b, Sargent & Filippenko 1991). The ratio between this line and the bump at around 4686 Å has been synthesized by Meynet (1995). The ratio we have measured,  $L(WR_{4686})/L(WR_{5808}) = 0.5$ , is also

consistent with the age constraints we have derived. It is interesting to note that the high value of this ratio can only be reproduced assuming enhanced mass-loss rates in the WR atmosphere (Meynet 1995). At the metallicity of NGC 4214, the peak in the WC/WR ratio is reached between 3 and 3.5 Myr.  $W(\text{Si IV})/W(\text{C IV})$  and  $W(H\beta)$  are simultaneous consistent with an age for the burst around 3 Myr. They furthermore constrain the IMF slope to a rather flat value close to  $\alpha = 3$ . This short discussion serves as an example of how the use of different parameters (WR bump,  $W(H\beta)$ ,  $W(\text{Si IV})/W(\text{C IV})$ ) allows to constrain uniquely the properties of the star formation episode. The fact that all they predict the same range of ages provides a strong reliability on the consistency of the method.

We want to remind here that the optical continuum is severely contaminated by an underlying population of older stars (see Fig. 5). Both  $W(H\beta)$  and  $W(WR_{bump})$  had to be corrected from this underlying continuum before comparison with the predictions of synthesis models. Otherwise, the results would not have been reliable. Indeed, without removal of the contamination it would have been impossible to fit all the parameters simultaneously. Moreover, in the case of extended regions like this one, special care has to be given to integrate properly the continuum from the young cluster and the emission lines originating in the whole extension of the gas ionized by the cluster. In this case, both the  $L(WR)/L(H\beta)$  and  $W(H\beta)$  corrected values we have used in the fitting have been taken from Maíz-Apellániz et al. (1998) and were obtained, integrating the whole  $H\beta$  emission associated to the star cluster, correcting from differential extinction and removing the optical continuum contribution from older stars. These authors have shown, for example, that the  $L(WR)/L(H\beta)$  value measured over an aperture of  $2'' \times 2''$  could be up to 25 times larger than the intrinsic value. This effect led Sargent & Filippenko (1991) to conclude erroneously that the WR population in this galaxy was abnormally high. Similarly, the value of the  $L(WR)/L(H\beta)$  ratio quoted by Meynet (1995) was obtained through a small aperture and is severely overestimated: it can't indeed be reproduced by any synthesis model.

The IMF slope we have derived coincides with the optimum value obtained by Leitherer et al. (1996) by fitting the profiles of the Si IV and C IV stellar absorption lines observed with HST. Although they derive a slightly older age (around 4 Myr), this good agreement provides an additional support for the validity of the assumptions we have made for using the  $W(\text{Si IV})/W(\text{C IV})$  ratio, as we have explained above.

NGC 4214 is one of the objects showing the largest discrepancy between the reddening derived from our continuum synthesis procedure and the extinction measured through the Balmer lines ratios ( $E(B - V) = 0.07$  vs. 0.28, respectively). As we have discussed above, Maíz-Apellániz et al. (1998) have mapped the distribution of stars, ionized gas and dust in this object, showing that the dust is concentrated at a certain distance from the stellar cluster, but still within the ionized nebula. As a result, the UV continuum comes out without being significantly affected by extinction, while the emission lines are strongly affected by dust. The quite large number of massive

stars formed have apparently wiped out the dust particles from their surroundings, leaving free paths through which the stellar continuum can emerge. We believe that this scenario could also be valid for other large star-forming regions affected by strong stellar winds.

We finally want to comment that the observed FIR luminosity is underestimated by the models, as expected since we know that there are several star-forming knots outside the aperture we have used for normalization, that still contribute to the IRAS measurements.

### 6.3. Mrk 59

Mrk 59 is a giant H II region located to the southern extreme of the irregular galaxy NGC 4861. Its UV spectrum shows a very steep continuum, indicating the absence of significant amounts of dust. The optical emission lines are also unaffected by reddening. The region is dominated by a strong burst having transformed around  $10^6 M_{\odot}$  of gas into stars some 3 Myr ago. The IMF seems to be rather steep, although its determination is rather inaccurate for this object. There is an important population of WR stars, as derived from the  $L(WR)/L(H\beta)$  ratio, which at the metallicity of this galaxy excludes the possibility of an extended star formation episode and constrains the ages to the range 3.0 - 4.5 Myr.

The global absolute magnitudes as  $L_{FIR}$  and  $L(H\beta)$  are well reproduced by the models (within 15%). It is interesting to note here that the predicted  $L_{FIR}$  is generated mainly by the absorption of Lyman continuum and Lyman  $\alpha$  photons, since the extinction affecting the continuum is very weak. The efficiency in the destruction of ionizing photons has been included in our models as a constant fraction of 30%, as discussed above. This efficiency controls both the resulting  $L_{FIR}$  and  $L(H\beta)$  values. The good agreement between predictions and observations allows us to rely on the efficiency we have assumed, at least for some individual cases. The good agreement with the observed FIR luminosity implies also that the burst is dominating the energetics of the whole region. This is also evident when comparing the predicted and observed optical continua. The contribution of any underlying older stellar population to the total optical continuum is negligible when compared to the burst emission.

### 6.4. IZw 18 (=Mrk 116)

IZw 18 is the prototype of an isolated low metallicity blue compact galaxy experiencing an intense episode of star formation. With a mean metallicity as low as  $Z = Z_{\odot} / 40$  (Searle & Sargent 1972) it constitutes an ideal laboratory to study the formation and evolution of massive stars at very low metal abundances, and has been studied extensively in the last years. Assuming a single instantaneous burst, Lequeux et al. (1981) concluded that the present star formation episode in IZw 18 is not older than 3 Myr, but noted that an extended burst during around 15 Myr would also be consistent with the observational data. Kunth, Matteucci & Marconi (1995) have analyzed the

chemical evolution of this metal deficient galaxy. Their models favour an extended star formation process active at least during the last 10-20 Myr, instead of a very young instantaneous episode. Martin (1996) has found an expanding shell of ionized gas around the massive stellar cluster. From the kinematics of this shell and from the analysis of chemical evolution models she concluded that massive stars have been forming continuously in IZw18 during the last 13 Myr. Finally, Hunter & Thronson (1995) have identified individual stars in IZw 18 with WFPC-2 on the Hubble Space Telescope. The picture emerging from their results is one in which star formation began some tens of Myr ago, especially in the central and northern part of the galaxy. Star formation should have continued since then throughout the rest of the galaxy in smaller star-forming events, giving rise to two main concentrations of massive stars, comprising around half of them, together with other stars scattered throughout the galaxy. The age estimated for the inner H $\alpha$  filaments span between 1 and around 10 Myr. An additional outer filament could be several tens of Myr old and is probably related to the onset of star formation in IZw 18.

Our models can reproduce the majority of the observational parameters either by assuming an instantaneous burst 3.0 Myr old, in agreement with Lequeux et al. (1981), or an extended star formation process with a constant SFR during the last 13 Myr. Considering the additional constraints imposed by the chemical evolution models and HST imaging, we have considered only the extended burst scenario. The onset of relatively small star formation events throughout the galaxy at a nearly constant rate would indeed mimic a continuous star formation process if analyzed globally, as we do through the large IUE aperture. The low metallicity of this object does not allow to measure the individual Si IV and C IV lines of stellar origin, so that we cannot constrain in any way the IMF slope. We have hence assumed a standard Salpeter IMF in our analysis.

Both the continuum and the emission lines are weakly reddened, with  $E(B - V)$  around 0.05 in both cases. Although at such low reddening our sensitivity to the shape of the extinction law is small, the best fit is obtained assuming the Galactic law ( $\epsilon = 0.06$ -Gal, 0.10-LMC, 0.12-SMC). We wonder therefore whether this reddening could be due to residual Galactic extinction, not completely corrected by the Burstein & Heiles (1984) method. The predicted FIR emission is very close to the limit of detectability of IRAS, explaining so its non-detection by this satellite. The predicted radio spectral index, mainly thermal, coincides well with the observational one (although the radio emission is underestimated by an order of magnitude). The synthetic H $\beta$  emission is also consistent with the value we measured and is essentially identical to the one derived from the HST observations by Hunter & Thronson (1995).

It can be seen in Fig. 5 that the synthetic continuum reproduces well both the observed UV and optical ranges, up to 7000 Å. There is no significant excess continuum in the optical as in other galaxies. We therefore conclude that the present burst of star formation is dominating the emission over the whole UV-optical range, and that the continuum associated to an underlying population if any is negligible. The contribution

from stars formed in a prior burst several tens of Myr ago, as postulated by Hunter & Thronson (1995), should therefore be very small (compared to the emission from the present burst), even in the optical range. Our conclusion is that while the H $\alpha$  filaments show that star formation could have begun in IZw 18 several tens of Myr ago, the global star formation rate should have increased significantly around 13 Myr ago, and has been maintained essentially constant since then.

Our models predict a very small number of WR stars in IZw 18, with  $WR/(WR+O) \approx 3 \cdot 10^{-4}$ . Legrand et al. (1997b) and Izotov et al. (1997) detected a small population of WR stars in this galaxy. While both groups agree that the optical bumps are due to at least some WC stars, the presence of WN ones is more controversial. Our models do not predict the presence of WC stars at such low metallicities, unless the formation of WR stars in binary systems is considered. Cerviño (1998) shows that even for a small fraction of stars evolving in binary systems, mass transfer allows the formation of WRs (mainly of WC type) at ages above around 6 Myr, in good agreement with our age estimates. On the other hand, models assuming enhanced mass loss also predict the formation of a small number of WC stars at very low metallicities (Schaerer & Vacca 1998), within a short time period of 1 Myr peaking at an age of 3 Myr. These predictions would be in agreement with the observations only if these stars have been formed within one of the very young clusters in IZw 18. A precise location of these stars would be required to disentangle which effect is dominating in this case: the formation of WRs via the binary channel, or enhanced mass loss rates (or both together!). Up to now, there is only a marginal detection with HST of 2 possible WR candidates by Hunter & Thronson (1995), and some evidences compatible with 5–9 WNL stars and/or compact nebular He II emission by de Mello et al. (1998).

Evolutionary models also predict a small number of red supergiant stars (RSG) at the metallicity of IZw 18, and indeed some individual K and MRSGs have been identified by Hunter & Thronson (1995). Cerviño & Mas-Hesse (1994) explained how current stellar evolutionary tracks predict smaller populations of RSGs the lower the metal abundance. The relatively blue  $V - K$  value measured by Thuan (1983) through a circular aperture  $8''$  in diameter ( $V - K = 0.57 \pm 0.23$ ) is well reproduced by our models ( $V - K \approx 0.5 \pm 0.1$  for an extended burst between 10 and 20 Myr old), thus supporting the predictions of current stellar tracks.

### 6.5. Haro 2 (=Mrk 33)

Haro 2 is one of the brightest blue compact galaxy in our sample. At a distance of 20.2 Mpc it has the shape and brightness profile of an elliptical galaxy but with a bright, blue nucleus containing an important number of WR stars (Kunth & Joubert 1985). At a metallicity 3 times lower than the Sun it shows clear stellar absorption lines in the UV range (Si IV and C IV). In the optical spectrum strong stellar absorption wings are also clearly visible around the Balmer emission lines. Recently, Lequeux et al. (1995) and Legrand et al. (1997a) have found evidences of

a strong outflow of gas having been ejected from the starburst region at velocities close to 200 km/s, around 1 Myr ago.

Fanelli et al. (1988) have analyzed the UV spectrum of Haro 2 using optimized, non-evolutionary, stellar synthesis techniques. These authors derived a strongly discontinuous luminosity function for this galaxy, with an important contribution to the UV emission of main sequence stars in the ranges O3-6 (46% at 1500 Å) and B1-2 (48%), as well as a marginal contribution from A0-2 stars (6%). The interstellar reddening affecting the UV continuum derived by this technique corresponds to  $E(B - V) = 0.15$  (assuming a Galactic-like extinction law). The strong contribution of the O3-6 group reveals the presence of an important population of young massive stars (less than 5 Myr old). From the discontinuities in the derived luminosity functions they concluded that the present burst of star formation has been preceded by at least two bursts, the most recent of which ended not more than 20 Myr ago giving an important contribution of B1-B2 stars. Our analysis, based on evolutionary synthesis techniques, yields an age of 4.5 Myr for the present burst, with best fits obtained for a rather steep IMF ( $\alpha \geq 3.0$ ) and a nearly instantaneous star-formation episode. Our fitting procedure yields an extinction law similar to the LMC one, with  $E(B - V) = 0.12$ . Both Galactic and SMC laws are excluded, with  $\epsilon$  parameters above 0.14, compared to  $\epsilon = 0.06$  for the LMC law. The age and extinction strength we derive are consistent with Fanelli et al. (1988) for the present burst. Nevertheless, our models naturally predict an important contribution to the UV continuum of stars with spectral types cooler than O6, with no need to invoke a discontinuous luminosity function. The discontinuity in the luminosity function found by the optimizing synthesis technique could be a consequence of adopting a Galactic-like extinction law, which we found unable to reproduce the observations in Haro 2.

On the other hand, our models clearly underestimate the optical continuum, as shown in Fig. 5. It seems that the stars formed in the present burst, the only ones to which our UV observables are sensitive, account for no more than 60% of the total optical emission. The shape of the optical continuum seems to be dominated by A stars which must have been formed in a previous much older burst. Our models correctly reproduce several other independent observables of Haro 2. We predict a relative population of WR stars  $WR/(WR+O) = 0.04$ , which can account for the observed WR features. The FIR emission is also well explained supporting the extinction value we have derived from our UV fitting procedure. The excess FIR emission is probably associated to the underlying stellar population, which, as we have shown, is significant in this galaxy. The total H $\beta$  emission is also satisfactorily reproduced within a factor 1.3, as well as the relatively low effective temperature. The  $WR/(WR+O)$  and  $T_{eff}$  values derived for this galaxy set indeed strong constraints against an extended star formation episode.

Our results are also consistent with the detection of outflowing gas cited above. As discussed by Lequeux et al. (1995), the gas should have been ejected from the central part of the galaxy around 1 Myr ago. This is consistent with a relatively

evolved, massive starburst, which begins to ignite supernovae after the first 3.5 Myr of evolution (assuming  $M_{up} \approx 120 M_{\odot}$ ). Since the mass transformed into stars in Haro 2 is rather high (more than  $6 \cdot 10^6 M_{\odot}$ ), the estimated number of supernova explosions in the first  $10^6$  yr after the most massive stars have exhausted their nuclear fuel has to be as high as 500-1000. The kinetic energy ejected by so many supernovae is large enough to power the outflowing wind. Moreover, such a strong release of energy could have blown away much of the gas left in the core of this galaxy, explaining the non-detection by Lequeux et al. (1995) of any neutral gas at the redshift of the starburst.

### 6.6. Mrk 710 (=NGC 3049)

Mrk 710 is the only large spiral galaxy with a starburst nucleus in our sample. It is furthermore one of the two objects with a metallicity as high as solar, to be compared with the properties of star-formation processes in metal-deficient blue compact galaxies. Mrk 710 is known to host an important population of more than 15000 WR stars (Kunth & Schild 1986, Vacca & Conti 1992). As expected for a starburst located within the bulge of a large galaxy, the relative contribution of the underlying population is very important. We can see in Fig. 5 that around 60% of the observed optical continuum emission is associated to this older population, whose contribution to the UV below 2000 Å is negligible. The measured  $W(H\beta)$  value has therefore to be corrected by a factor of 2.5, in order to derive the value intrinsically associated to the present starburst. An additional correction for differential extinction was also applied, yielding a final  $W(H\beta)$  value almost a factor of 3 higher than the observed one.

The observational parameters of Mrk 710 can be in general well reproduced by an instantaneous episode of star formation, around 3.5 Myr old, with an IMF somewhat flatter than Salpeter one. The predicted WR stars population, with  $WR/(WR + O) = 0.06$ , reproduces well the observed WR features. The large  $L(WR)/L(H\beta)$  ratio is indeed consistent with the prediction for solar metallicity stars. It cannot be reproduced by extended star formation models and constrains the episode to have been essentially instantaneous. On the other hand, the effective temperature derived from the optical emission lines is clearly underestimated by the models. The origin of this discrepancy could be the presence of some WR stars with effective temperatures higher than those predicted by current evolutionary tracks. There are indeed observational evidences that some WR stars can reach  $T_{eff}$  values above  $10^5$  K. If some of them are present, they could dominate the shape of the integrated ionizing continuum. On the other hand, the detection of the OI  $\lambda 6300$  Å line in this galaxy indicates that shocks are affecting the ionization process so that the  $T_{eff}$  values derived assuming pure photoionization might be overestimated. Due to its high metallicity, Mrk 710 shows also the strongest Si IV and C IV absorption lines in our sample, supporting the correlation between the equivalent widths of these lines and the nebular metal abundance we have plotted in Fig. 3.

Despite the close to solar metallicity of this galaxy, the extinction affecting the UV continuum differs significantly from the Galactic extinction law. We show in Fig. 14 the synthetic continuum optimally reddened by using three possible laws. It can be seen that reasonable fits are achieved only by using the LMC or SMC laws, with the best fit obtained with the LMC one for  $E(B - V) = 0.17$ . The Galactic law is completely excluded. The FIR luminosity is underestimated by 30%, as expected in this galaxy where the IRAS data are integrated over a much larger region than the IUE flux, and include the whole nucleus and the spiral arms. Nevertheless, the fact that the observed FIR luminosity is within a factor 1.3 of the predicted one indicates that the starburst in the nucleus of this galaxy is the most powerful source of energy dominating over other possible individual star formation episodes in the spiral arms.

The mass of gas transformed into stars is close to  $10^6 M_{\odot}$ . While this amount of mass is clearly higher than in Giant H II regions in spiral arms, it is similar to the values derived in some blue compact galaxies. We conclude therefore that there are no significant differences between the bursts observed in relatively small, metal deficient, structureless galaxies, like BCGs, and the episodes taking place in the nuclei of large metal-rich spiral galaxies such as Mrk 710.

### 6.7. NGC 3256

NGC 3256 has been classified as the remnant of two colliding galaxies, on the basis of its tidal tails and highly chaotic nuclear region (Graham et al. 1984). Joseph & Wright (1985) concluded that such a merger would produce a burst of star formation of exceptional intensity, what they called a “super starburst”. The detection of strong Si IV and C IV absorption lines by Joseph et al. (1986) is clearly indicative of the presence of massive stars. Moorwood & Oliva (1994) have mapped the spatial distribution of several near infrared lines, finding that Br $\gamma$  is extended over a  $26'' \times 13''$  region. Doyon, Joseph & Wright (1994) have detected a large number of red supergiants in the central part of the galaxy, constraining the age of the starburst to between 12 and 27 Myr, assuming continuous star formation episodes with different decaying star formation rates. We included this galaxy in our sample for comparison to analyze the properties of a very intense episode of star formation in a dusty medium and induced by a merging process.

The UV continuum and  $W(H\beta)$  value are best reproduced by a rather evolved cluster around 5 Myr old, in a very dusty environment ( $E(B - V) = 0.16$  for an SMC law) and with an IMF slope close to Salpeter one. The derived amount of gas transformed into stars is indeed very large,  $M > 10^7 M_{\odot}$  and the measured extinction is significantly larger than in normal blue compact galaxies. It is interesting to note that in Mrk 710 and NGC 3256, the two galaxies with higher metallicity and the more affected by reddening in our sample, the extinction seems to follow LMC or SMC laws characterized by a weak bump at 2175 Å, supporting our conclusion that there is no correlation between metallicity and the shape of the extinction law.

While our models correctly reproduce the observed UV continuum, they significantly underestimate the total FIR emission, as well as the total  $H\beta$  luminosity by almost an order of magnitude. Moreover, at an age around 5 Myr the cluster would be too young to host the significant number of RSGs found there. The large extinction suggests that a significant number of massive stars could be completely hidden by dust, so that while their contribution to the UV continuum would be negligible, almost all their emission would be reradiated in the FIR range. Their ionizing flux could also contribute to the  $Br\gamma$  emission observed in the near infrared, as well as to the Balmer lines emission. If this is the case, our analysis would correspond to only a group of massive stars which happen to be less affected by extinction than the bulk of the cluster, so that the results can not be extrapolated to the starburst as a whole. The mass of stars derived by Doyon et al. (1994) from the near infrared lines is indeed also a factor of 10 larger than the mass we derive from the UV continuum flux, supporting the idea that only a fraction of the stars are visible in the UV. This scheme is also favoured by the fact that the extinction derived from the Balmer decrement is much larger than the value derived from UV continuum fits ( $E(B - V) = 0.85$  vs. 0.16, respectively). While no contribution at all is expected from the hidden stars in the UV, we would expect some contribution from the obscured regions at  $H\alpha$  wavelengths, yielding a large global Balmer decrement.

We conclude that starbursts taking place in dusty regions of merging galaxies can have a rather different appearance from those of BCGs: flat UV continua due to the strong extinction, reddened emission lines, hidden massive stars, etc... These are the properties expected for the starburst powering ultraluminous IRAS galaxies, in several of which the UV continuum could even not be detected. Nevertheless, the intrinsic properties of the star formation processes are similar to those of the dust-free weaker bursts observed in other objects.

## 7. Conclusions

We have analyzed the properties of the star formation episodes taking place in a sample of blue compact and irregular galaxies. We have applied our evolutionary population synthesis models to a multiwavelength data set, including independent UV, optical, FIR and radio parameters related to different physical processes. Comparing the predicted with the observational values of the different parameters we have been able to constrain the age, the star formation regime (instantaneous or extended) and the Initial Mass Function slope of the massive star formation processes powering these galaxies, as well as the shape and strength of the interstellar extinction affecting them. We summarize our main results as follows:

- Formation of massive stars proceeds by episodic, very short bursts, so that the stars can be considered to be essentially coeval. Nevertheless, the superposition of several of these short bursts at different times could mimic in some cases a star formation process extended during several million years when the integrated emission from an object is analyzed.
- Massive star clusters with nearly instantaneous bursts have ages below 5-6 Myr with an average around 3.5 Myr. Older bursts would not produce enough ionizing flux to be detected as emission line galaxies. Powerful IRAS galaxies might be Postburst Galaxies, characterized by a strong FIR emission with very weak emission lines.
- Despite the large range in the number of stars formed and the amount of gas transformed (covering 4 orders of magnitude) the derived IMF shows a slope in average very close to the solar neighbourhood value. The IMF does not seem to depend onto the various star formation scenarios in objects as different as giant H II regions, BCGs, starburst nuclei and merging galaxies. We have found no correlation between the deviations from this mean value and the metallicity, morphology or interaction state of these galaxies.
- Emission associated to these starbursts completely dominates the UV, optical and FIR ranges, indicating that the present bursts might have been one of the strongest in their history or in some cases the first global episode of massive star formation. In some galaxies however the contribution of the young stars to the optical continuum is comparable to the emission associated to older stars formed in preceding bursts.
- No starbursts have been found with  $W(H\beta)$  as high as predicted by the models for the first 2 Myr after massive star have been formed, despite the evidences that stars with initial masses close to  $100 M_{\odot}$  form in these galaxies with an IMF slope similar to that of the solar neighbourhood. The fact that already during accretion stars more massive than  $40 M_{\odot}$  might burn a substantial fraction of its central hydrogen could lead to smaller effective temperatures and ionizing powers in the first 2 Myr, possibly explaining so this effect.
- Low mass stars formation should take place in these regions before the most massive stars ignite, and wouldn't be therefore strictly coeval to them. Otherwise, they would end their slow collapse when the most massive stars are already evolved and the ionizing flux of the cluster has almost completely faded, not being any longer recognized as a starburst.
- The observed population of Wolf-Rayet stars is well reproduced by current models. The detection of large  $WR/(WR + O)$  ratios is the strongest indication of a short duration star formation episode.
- The relatively blue  $V - K$  colors measured in IZw 18, which has been forming massive stars during several Myr, confirms the predictions of current stellar evolutionary tracks that very few red supergiants would be formed at low metallicities.
- A relatively large number of supernova explosions (up to 1 per 100 years) is expected to take place in these compact regions. Thousands of supernova remnants have to be present in the most evolved of these starbursts. The release of kinetic energy and the ejection of metals must severely disturb the interstellar gas producing bubbles and metal enriched outflowing winds.

- The good agreement between observed and predicted FIR luminosities excludes in general the possibility that a significant number of massive stars could be hidden within UV-optical opaque clouds, although this probably happens in some individual objects.
- The extinction follows a law similar to the LMC and SMC ones, with a very weak absorption bump at 2175 Å, if any. There is no dependence between the shape of the extinction law and the metallicity or the size of the regions, indicating that the strong radiation associated to the burst has destroyed the dust components responsible for the UV bump. We find no need to invoke a specific extinction law other than the LMC or SMC ones.
- The strength of the extinction derived from the Balmer decrement is in many cases larger than the one obtained from the UV continuum. While the contamination by strong stellar absorption lines, with equivalent widths around 4-5 Å could explain the discrepancy in some cases, it is more likely related to the inhomogeneous distribution of stars, ionized gas and dust. Dust particles concentrate along patchy structures far away from the continuum sources, but still within the ionized gas, affecting more the emission lines than the continuum. The trend toward higher values of the nebular extinction, the more evolved the regions, suggests that the newly formed dust grains are ejected far away from the progenitor stars.

*Acknowledgements.* We wish to thank M. Cerviño for his help in the development of the synthesis models. JMMH is grateful for the hospitality of the Institut d'Astrophysique de Paris, where part of this work has been performed. We are grateful for the support provided by the staff of the VILSPA-IUE, Nançay and Roque de los Muchachos (La Palma island) observatories. We wish to particularly thank the collaboration by L. Bottinelli and L. Gouguenheim for performing the observations at Nançay. We are grateful to M. Rosa and S. D'Odorico who provided to us their spectrum of NGC 5471. Extensive use of the NASA Extragalactic Database is also acknowledged. This work has been partially financed through different grants from Spanish CI-CYT (ESP95-0389-C02-02) and from the Spanish-French PICASSO program.

## References

- Aaronson M., Mould J. 1983, ApJ, 265, 1  
 Allen D.A., Wright A.E., Goss W.M. 1976, MNRAS, 177, 91  
 Alloin D., Sareyan J.-P. 1974, A&A, 33, 331  
 Alloin D. 1974, A&A, 33, 337  
 Arnault Ph., Kunth D., Schild H. 1989, A&A, 224, 73  
 Beck S.C., Turner J.L., Ho P.T.P., Lacy J.H., Kelly D.M. 1996, ApJ, 457, 610  
 Bernasconi P.A., Maeder A. 1996, A&A, 307, 829  
 Blitz L., Israel F.P., Gatley I., Lee T.J., Beattie D.H. 1981, ApJ, 249, 76  
 Buat V., Deharveng J.M. 1988, A&A, 195, 60  
 Burstein D., Heiles C. 1984, ApJ, 54, 33  
 Calzetti D., Kinney A.L., Storchi-Bergmann T. 1994, ApJ, 429, 582  
 Calzetti D., Bohlin R.C., Kinney A.L., Storchi-Bergmann T., Heckman T.M. 1995a, ApJ, 443, 136  
 Calzetti D., Kinney A.L., Storchi-Bergmann T. 1996, ApJ, 458, 132  
 Campbell A., Terlevich R., Melnick J. 1986, MNRAS, 223, 811  
 Caplan J., Deharveng L. 1986, A&A, 155, 297  
 Cardelli J.A., Clayton G.C., Mathis J.S. 1989, ApJ, 345, 245  
 Charbonnel C., Meynet G., Maeder A., Schaller G., Schaerer D. 1993, A&AS, 101, 415  
 Cerviño M., Mas-Hesse J.M., 1994, A&A, 284, 749  
 Cerviño M. 1998, Ph. D., Universidad Complutense de Madrid  
 Conti P. 1991, ApJ, 377, 115  
 Copetti M.V.F., Pastoriza M.G., Dottori H.A. 1985, A&A, 152, 427  
 De Mello D.F., Schaerer D., Heldmann J., Leitherer C. 1998, ApJ, in press  
 Díaz A. 1988, MNRAS, 231, 57  
 Doyon R., Joseph R. D., Wright G. S. 1994, ApJ, 421, 101  
 Fanelli M.N., O'Connell R.W., Thuan T.X., 1988, ApJ, 334, 665  
 French H.B. 1980, ApJ, 240, 41  
 Forbes D.A., Ward M.J. 1993, ApJ, 416, 150  
 García-Vargas M-L., Díaz, A.I. 1994, ApJS, 91, 553  
 Gordon K.D., Calzetti D., Witt A.N. 1997, ApJ, 487, 625  
 Graham J.R., Wright G.S., Meikle W.P.S., Joseph R.D. 1984, Nature, 310, 213  
 Griffiths R.E., Della Ceca R., Georgantopoulos I., Boyle, B.J., Stewart, G.C., Shanks, T., Fruscione A. 1996, MNRAS, 281, 71  
 Heckman T.M., Robert C., Leitherer C., Garnett D.R., Van Der Rydt F. 1998, ApJ, 503, 646  
 Helou G., Khan I.R., Malek L., Boehmer, L. 1988, ApJS, 68, 151  
 Heydari-Malayeri M., Melnick J., Martin J.M. 1990, A&A 234, 99  
 Heydari-Malayeri M. 1996, The Interplay between Massive Star Formation, the ISM and Galaxy Evolution, ed. D. Kunth, B. Guiderdoni, M. Heydari-Malayeri, T.X. Thuan (Editions Frontières), 51  
 Huchra J.P., Geller M.J., Gallagher J., Hunter D., Hartmann L., Fabiano G., Aaronson M. 1983, ApJ, 274, 125  
 Hunter D.A., Thronson H.A. 1995, ApJ, 452, 238  
 Hunter D.A., Gillett F.C., Gallagher J., Rice, W.L., Low F.J. 1986, ApJ, 303, 171  
 Israel F.P., Kennicutt R. C. 1980, Astrophysical Letters, 21, 1  
 Izotov Y.I., Foltz C.B., Green R.F., Guseva N.G., Thuan T.X. 1997, ApJ, 487, L37  
 Joseph R.D., Wright G.S. 1985, MNRAS, 214, 87  
 Joseph R.D., Wright G.S., Prestwich A.H. 1986, in New Insights in Astrophysics. Eight Years of UV Astronomy with IUE, 597  
 Keel W.C. 1993, AJ, 106, 1771  
 Kinman T.D., Davidson K. 1981, ApJ, 243, 127  
 Kinney A.L., Bohlin R.C., Calzetti D., Panagia N., Wyse R.F.G. 1993, ApJS, 86, 5  
 Kinney A.L., Calzetti D., Bohlin R.C., McQuade K., Storchi-Bergmann Th., Schmitt H.R. 1996, ApJ, 467, 38  
 Klein U., Wielebinski R., Thuan T.X. 1984, A&A, 141, 241  
 Kondo Y. 1988, Exploring the Universe with the IUE Satellite, Dordrecht:Reidel  
 Koornneef J. 1993, ApJ, 403, 581  
 Kühr H., Witzel A., Pauliny-Toth I.I.K., Nauber U. 1981, A&AS, 45, 367  
 Kunth D., Sargent W.L.W. 1981, A&A, 101, L5  
 Kunth D., Sargent W.L.W. 1983, ApJ, 273, 81  
 Kunth D., Joubert M. 1985, A&A, 142, 411  
 Kunth D., Sèvre F. 1986, Star-forming Dwarf Galaxies and related Objects, eds. D. Kunth, T.X. Thuan and J. Tran Thanh Van (Editions Frontières)  
 Kunth D., Schild H. 1986, A&A, 169, 71  
 Kunth D., Matteucci F., Marconi G. 1995, A&A, 297, 634

- Kunth et al. 1996, *The Interplay between Massive Star Formation, the ISM and Galaxy Evolution*, eds. D. Kunth, B. Guiderdoni, M. Heydari-Malayeri, T.X. Thuan (Editions Frontières)
- Legrand F., Kunth D., Mas-Hesse J.M., Lequeux, J. 1997a, *A&A*, 326, 929
- Legrand F., Kunth D., Roy J.-R., Mas-Hesse J.M., Walsh J.R. 1997b, *A&A*, 326, 17L
- Leitherer C., Lamers, H.J.G.L. 1991, *ApJ*, 373, 89
- Leitherer C., Heckman T.M. 1995, *ApJS*, 96, 9
- Leitherer et al. 1996, *From Stars to Galaxies: the Impact of Stellar Physics on Galaxy Evolution*, ed. C. Leitherer, U. Fritze von Alvensleben, J. Huchra, (San Francisco: ASP)
- Lequeux J., Maucherat-Joubert M., Deharveng J.M., Kunth D. 1981, *A&A*, 103, 305
- Lequeux J., Kunth D., Mas-Hesse J.M., Sargent, W.L.W. 1995, *A&A*, 301, 18
- McCall M.L., Rybski, P.M., Shields G.A. 1985, *ApJS*, 57, 1
- Maeder A., Meynet G. 1994, *A&A*, 287, 803
- Maíz-Apellániz J., Mas-Hesse J.M., Muñoz-Tuñón C., Vílchez J.M., Castañeda, H.O. 1998, *A&A*, 329, 409
- Martin C.L. 1996, *ApJ*, 465, 680
- Mas-Hesse J.M. 1990, Ph. D., Universidad Complutense de Madrid
- Mas-Hesse J.M., Kunth D. 1991a, *A&AS*, 88, 399
- Mas-Hesse D., Kunth D. 1991b, in *IAU Symp 143, Wolf-Rayet Stars and Interrelations with other Stars in Galaxies*, ed. K. van der Hucht, B. Hydayat (Dordrecht:Kluwer), 613
- Mas-Hesse J.M. 1992, *A&A*, 253, 49
- Mas-Hesse J.M., Muñoz-Tuñón C., Vílchez J.M., Castañeda, H.O., Carter D. 1994, in *Violent Star Formation: From 30 Dor to QSOs*, Ed. G. Tenorio-Tagle, (Cambridge:CUP), 125
- Mas-Hesse J.M., Kunth D. 1996a, in *The Interplay between Massive Star Formation, the ISM and Galaxy Evolution*, ed. D. Kunth, B. Guiderdoni, M. Heydari-Malayeri, T.X. Thuan (Editions Frontières), 401
- Mas-Hesse J.M., Kunth D. 1996b, in *From Stars to Galaxies: the Impact of Stellar Physics on Galaxy Evolution*, ed. C. Leitherer, U. Fritze von Alvensleben, J. Huchra, (San Francisco: ASP), 69
- Massey P., Lang C.C., Degioia-Eastwood, K., Garmany C.D. 1995, *ApJ*, 438, 188
- Mazzarella J.M., Balzano V.A. 1986, *ApJS*, 62, 751
- McQuade K., Calzetti D., Kinney A.L. 1995, *ApJS*, 97, 331
- Melnick J. 1979, *ApJ*, 228, 112
- Melnick J., Terlevich R., Eggleton P. P. 1985, *MNRAS*, 216, 255
- Meier D.L., Terlevich R. 1981, *ApJ*, 246, L109
- Mezger P.O. 1978, *A&A*, 70, 565
- Mezger P.G., Mathis J.S., Panagia N. 1982, *A&A*, 105, 372
- Meynet G. 1995, *A&A*, 298, 767
- Moorwood A.F.M., Oliva E. 1994, *ApJ*, 429, 602
- Nandy K., Morgan D.H., Willis A.J., Wilson R., Gondhalekar, P.M. 1981, *MNRAS*, 196, 955
- Olofsson K. 1995, *A&AS*, 111, 57
- Osterbrock D.E. 1989, *Astrophysics of Gaseous Nebulae and Active Galactic Nuclei*, (Mill Valley,CA:University Science Books)
- Peimbert M., Peña M., Torres-Peimbert S. 1986, *A&A*, 158, 266
- Prévot M.L., Lequeux J., Prévot L., Maurice E., Rocca-Volmerange B. 1984, *A&A*, 132, 389
- Puget J.L., Léger A. 1989, *ARA&A*, 27, 161
- Robert C., Leitherer C., Heckman T.M. 1993, *ApJ*, 418, 749
- Roy J.-R., Aube M., McCall M. & Dufour R.J., 1992, *ApJ*, 386, 498
- Rosa M., Joubert M., Benvenuti, P. 1984, *A&AS*, 57, 361
- Rosa M.R., Benvenuti P. 1994, *A&A*, 291, 1
- Saha A., Sandage A., Labhardt L., Schwengeler H., Tamman G.A., Panagia N., Machetto F.D. 1995, *ApJ*, 438, 8
- Sandage A., Tamman G.A. 1974a, *ApJ*, 190, 525
- Sandage A., Tamman G.A. 1974b, *ApJ*, 194, 559
- Sandage A., Bedke J. 1985, *AJ*, 90, 1992
- Sargent W.L.W., Filippenko A.V. 1991, *AJ*, 102, 107
- Scalo J. 1986, *Fundamentals of Cosmic Physics*, 11, 1
- Scalo J. 1990, in *Windows on Galaxies*, ed. G. Fabbiano et al., (Dordrecht:Kluwer)
- Schaerer D., Meynet G., Maeder A., Schaller, G. 1993a, *A&AS*, 98, 523
- Schaerer D., Charbonnel C., Meynet G., Maeder A., Schaller G. 1993b, *A&AS*, 102, 339
- Schaerer D. 1996, *ApJ*, 467, L17
- Schaerer D., Vacca W.D. 1998, *ApJ*, 497, 618
- Schaerer D., Contini Th., Pindao M. 1999, *A&AS*, in press
- Schaller G., Schaerer D., Meynet G., Maeder A. 1992, *A&AS*, 96, 269
- Searle L., Sargent W.L.W. 1972, *ApJ*, 173, 25
- Seaton M.J. 1979, *MNRAS*, 187, 73
- Sekiguchi K., Anderson K.S. 1987a, *AJ*, 94, 129
- Sekiguchi K., Anderson, K.S. 1987b, *AJ*, 94, 644
- Skillman E.D., Israel F.P. 1988, *A&A*, 203, 226
- Smith L.F., Mezger P.G., Biermann P. 1978, *A&A*, 66, 65
- Sramek R.A., Weedman D.W. 1986, *ApJ*, 302, 640
- Storchi-Bergmann T., Calzetti D., Kinney A.L. 1994, *ApJ*, 429, 572
- Storchi-Bergmann T., Kinney A.L., Challis P. 1995, *ApJS*, 98, 103
- Tenorio-Tagle G. 1994, in *Violent Star Formation: From 30 Dor to QSOs*, Ed. G. Tenorio-Tagle, (Cambridge:CUP), 50
- Tenorio-Tagle G., Muñoz-Tuñón C., Perez E., Melnick J. 1997, *ApJ*, 490, L179
- Terlevich R., Melnick J., Masegosa J., Moles M., Copetti M.V.F. 1991, *A&AS*, 91, 285
- Thuan T.X. 1983, *ApJ*, 268, 667
- Torres-Peimbert S., Peimbert M., Fierro J. 1989, *ApJ*, 345, 186
- Vacca W.D., Conti P.S. 1992, *ApJ*, 401, 543
- Van der Hucht K. et al. 1998, *Wolf-Rayet Phenomena in Massive Stars and Starburst Galaxies*, eds. K. Van der Hucht, G. Königsberger, Ph. Eenens, (San Francisco:ASP), in press
- Van Driel W., van den Broek A.C., de Jong T. 1991, *A&AS*, 90, 55
- Viallefond F., Thuan T.X. 1983, *ApJ*, 269, 444
- Viallefond F. 1986, in *Star-Forming Dwarf Galaxies and Related Objects*, eds. D. Kunth, T.X. Thuan, J. Tran Thanh Van, (Paris:Frontières), 207
- Vílchez J.M., Pagel B.E.J. 1988, *MNRAS*, 231, 257
- Wynn-Williams C.G., Becklin E.E. 1986, *ApJ*, 308, 260
- Zinnecker H. 1996, in *The Interplay between Massive Star Formation, the ISM and Galaxy Evolution*, ed. D. Kunth, B. Guiderdoni, M. Heydari-Malayeri, T.X. Thuan (Editions Frontières), 249